240 (2024) 213087

Contents lists available at ScienceDirect

Geoenergy Science and Engineering

journal homepage: www.sciencedirect.com/journal/geoenergy-science-and-engineering

Genetically linked litho- and organo-facies in meter-scale cycles of lacustrine deposits within the Permian Lucaogou Formation in the Bogda Mountains, Northwest China: Implications for paleoenvironment and organic matter origin

Xin Zhan [a,b,*], Wan Yang [b,**], Qiao Feng [c], Zhao-Wen Zhan [d], Sile Wei [e], Yujiao Zhang [f], Hongquan Kang [a], Tao Cheng [a], Hongyan Zhao [a], Wenjie Cai [a]

[a] CNOOC International Limited, Beijing, 100027, PR China
[b] Geology and Geophysics Program, Missouri University of Sciences and Technology, Rolla, MO 65409, USA
[c] College of Geoengineering and Geoinformatics, Shandong University of Science and Technology, Qingdao, 310003, PR China
[d] State Key Laboratory of Organic Geochemistry, Guangzhou Institute of Geochemistry, Chinese Academy of Sciences, Guangzhou, 510640, PR China
[e] School of Geosciences, Yangtze University, Wuhan, 430100, PR China
[f] National Center for Science and Technology Evaluation, Beijing, 100081, PR China

ARTICLE INFO

Keywords:
Lacustrine system
High-order cycles
Lithofacies and organofacies
Cyclostratigraphy
Chemostratigraphy
Biomarkers

ABSTRACT

A close correlation between lithofacies and organofacies in meter-scale high-order cycles composed of lacustrine sediments enables comparison and refinement of lithofacies-defined cyclostratigraphy. Four lithofacies and four organofacies have been identified in fluctuating profundal high-order cycles in the lower-Permian Lucaogou Formation, southern Bogda Mountains, NW China. The four lithofacies include interbedded and interlaminated coarse siltstone and very fine sandstone, black shale, wackestone and dolostone, and calcareous and dolomitic shales. Four distinctive organofacies have been identified, on the basis of geochemical composition of organic matter and specific biomarker proxies related to organic matter types, rather than to depositional conditions and thermal maturity. The four organofacies are associated with the four lithofacies in the meter-scale high-order cycles, suggesting litho- and organo-facies may be genetically linked and may have been controlled by lake contraction and extension. The study shows that the lithofacies-derived and environment-defined high-order cycles can be delineated and substantiated by geochemical proxies-defined organofacies. This study also demonstrates that a holistic approach combining litho- and organic geochemical data is useful in reconstruction of meter-scale lacustrine cycles in a half-graben.

1. Introduction

Lacustrine system, form in topographic lows, is an inland body of standing water occupying a depression, displaying high diversity, as they vary in size, morphology, water chemistry, formation, and seasonal variances among other factors (Gierlowski-Kordesch and Kelts, 1994). One lacustrine sequence-stratigraphic model is not applicable to all lake-basin types, because bewildering sedimentary process, respond-record, and intereactions portend a large complexity in ancient heterogeneous lake deposits, as the lake systems are sensitive to changing lake level and sediment supply, under control of accommodation and climate (Bohacs et al., 2000). The complexity of ancient lacustrine deposits can be studied effectively through combined sedimentological and geochemical investigations (e.g., Bradley, 1925; Carroll et al., 1992; Meyers, 1997; 2003), especially when linking lithofacies and geochemical facies in a stratigraphic framework (Bohacs et al., 2000).

Lithofacies is a mappable subdivision of a stratigraphic unit that can be distinguished by lithologic features (including both physical and organic characteristics) and sedimentary environment that produced it (Moore, 1949; AGI, 1973). Ancient lacustrine lithofacies may have unique geochemical imprints. For example, Curiale and Lin (1991)

* Corresponding author. CNOOC International Limited, Beijing, 100027, PR China.
** Corresponding author.
E-mail addresses: zhanxin@cnoocinternational.com (X. Zhan), yangwa@mst.edu (W. Yang).

https://doi.org/10.1016/j.geoen.2024.213087
Received 29 January 2023; Received in revised form 8 April 2023; Accepted 24 June 2024
Available online 27 June 2024

demonstrated that sediments in Tertiary deltaic and lacustrine environments, Montana, west-central North America contain different organic facies, in terms of organic matter types. Organofacies is subdivision of a rock body, which can be distinguished from adjacent subdivisions, through organic geochemical characteristics of the sediments, without considering the aspects of the inorganic fraction (Jones and Demaison, 1982). For instance, Mello et al. (1988) used biomarkers (e.g., gammacerane) that are sensitive to lakewater salinity to define organofacies of the Lower Cretaceous source rocks in Brazil, and to differentiate shales deposited in freshwater from saline lakes. Noteworthy, the application of organic geochemical proxies in environmental interpretations is effective within a time-stratigraphic framework (Horsfield et al., 1994; Carroll, 1998; Bohacs et al., 2000; Slatt and Rodriguez, 2012). A classification of lake-basin types in a sequence-stratigraphic-geochemical framework have also been established (Carroll and Bohacs, 1999, 2001; Bohacs et al., 2000). These authors have attempted to use a holistic approach linking lithofacies associations with organic geochemical facies/indicators in their lake type classification at a stratigraphic resolution of 10-1000 m scale. However, higher-resolution investigations at a cm-m scale on relationships between litho- and organo-facies are limited. The meter-scaled cycles are commonly recognized in the outcrop observations and

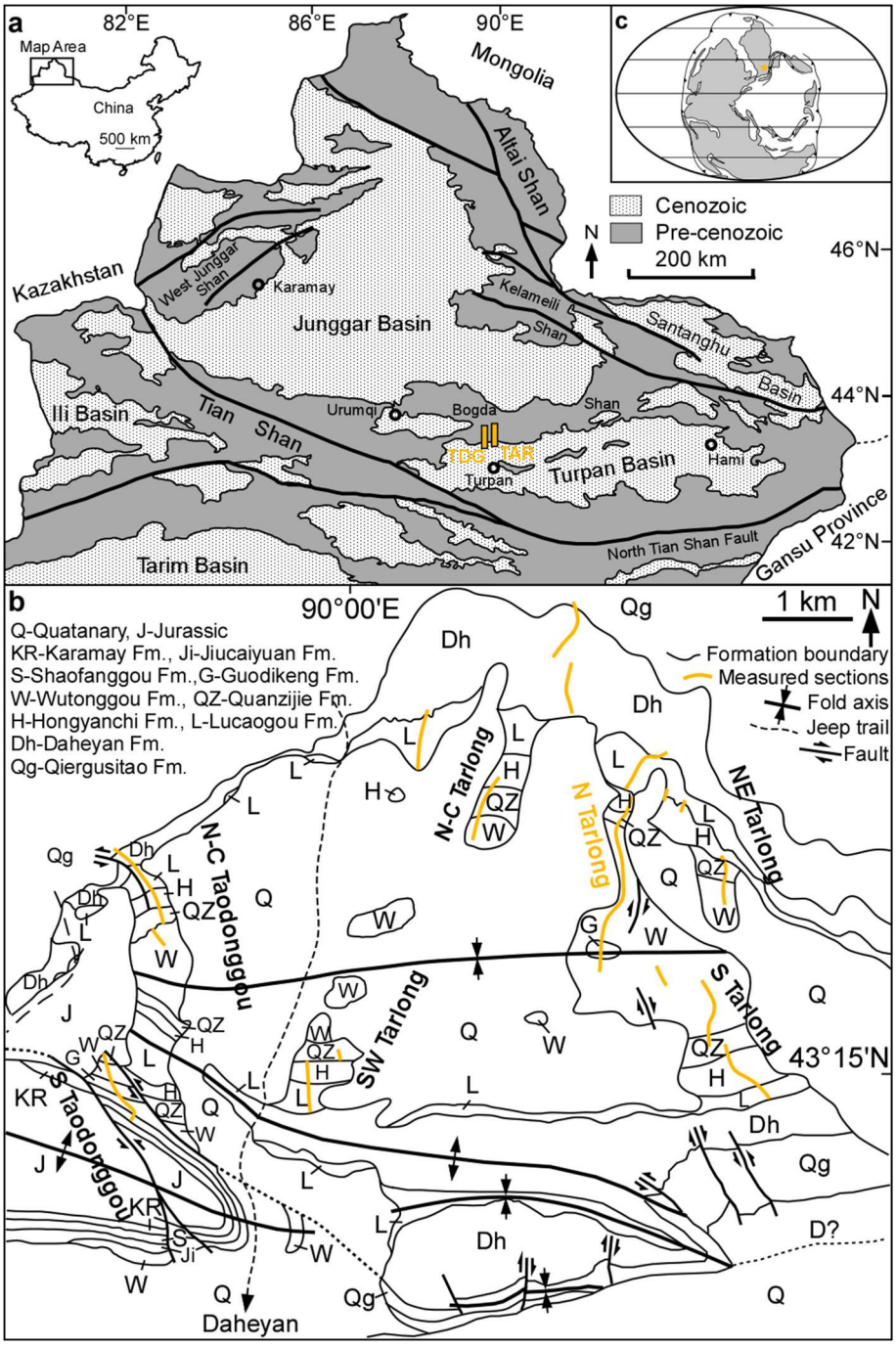

Fig. 1. (a) Geological map of the Turpan-Hami Basin, Junggar Basin, Santanghu Basin, Bogda Mountains, and Tianshan in Xinjiang Uygur Autonomous Region, NW China. Orange boxes show the location of Tarlong (TAR) and Taodonggou (TDG) sections. Modified from Chen et al. (1985), XBGMR (1993), and Yang et al. (2010). (b) Geological map of Tarlong-Taodonggou half-graben. Modified from Yang et al. (2010). (c) Paleotectonic and paleogeographic reconstruction of Pangea at early Permian (290 Ma) of Scotese (2014).

regarded as basic cyclostratigraphic entities, providing a framework to facilitate interpretations of sedimentary processes and their controlling factors (Yang et al., 2010). As a result, the complexity and variability of a lacustrine system can be better understood, with more accurate interpretation of lacustrine deposits at a smaller timescale.

Many previous studies on lithofacies or organofacies of lacustrine shales have been conducted in the lower Permian Lucaogou Formation, NW China, where cyclic siliciclastic and carbonate deposits are well exposed. These studies mainly focus on the depositional environment and organic matter accumulation of the Lucaogou shales, through petrology and mineralogy (Zhang and Li, 2018; Yang et al., 2019; Zhang et al., 2019, 2021; Liu et al., 2020, 2022), organic petrology and geochemistry (Hackley et al., 2016; Qiu et al., 2016; Liu et al., 2017, 2018; Su et al., 2019), and chemo-sedimentary facies and chemostratigraphy (Carroll, 1998; Bohacs et al., 2000; Liu et al., 2019a, 2019b; Meng et al., 2022; Tao et al., 2022). However, none of them investigate lacustrine cycles at a m scale. Exceptionally, alluvial-to-lacustrine depositional cycles of the Lucaogou deposits at a cm-m scale have been revealed through field observation, but without geochemical analysis (Yang et al., 2010; Olariu et al., 2022). In essence, few studies focus on the relationship between lithofacies and organofacies of cyclic deposits at a m scale. A rare case study of high-frequency redox variations of the Eocene cyclic lacustrine sediments at a m scale, based on geochemical evidences, has been reported in the western Qaidam Basin, China (Jiang et al., 2019), but lack of organofacies study.

This study investigates the relationship between litho- and organofacies of lacustrine deposits in high-order cycles at a meter-scale in the Lucaogou Formation in NW China, through detailed mineralogical, petrological, and geochemical characterization. It is the first work conducted that provides a higher-resolution change of litho- and organofacies of lacustrine deposits at a cm-m scale, with a practical method of combination of lithological and organic geochemical data, in order to advance the understanding of climatic and depositional processes on cyclic depositions at a 10^3–10^4 yr scale. The methodology of this study is useful for delineating highly variable depositional sequence of a lacustrine depositional system and predicting hydrocarbon distribution and characteristics in other partitioned basins.

2. Geological setting

The lacustrine deposits in the Lucaogou Formation of this study is exposed in Tarlong-Taodonggou area, which is ~15 km in the north of Daheyan at the southern foothills of Bogda Mountains, in the Turpan-Hami Basin of NW China (Fig. 1a). The Junggar and Turpan-Hami Basins, as one of the largest petroliferous basins in China, are of great interests to researchers who have been working on the Late Paleozoic continental deposits (Carroll and Bohacs, 1999, 2001; Hackley et al., 2016; Olariu et al., 2022). As a northeastern branch of the Tianshan Mountains, the Bogda Mountains separate the Turpan-Hami Basin to the south and from the Junggar Basin to the northwest (Fig. 1a). The Bogda Mountains were uplifted by strong intracontinental collision between the north Junggar Block and the south Tarim Block during Permian, forming a giant anticline that contains Devonian to Quaternary sedimentary and igneous rocks (Zhang, 1981; Wang et al., 2018). Carboniferous-Triassic fluvial-lacustrine deposits are exposed in syncline-anticline structures in the Tarlong and Taodonggou sections, in a half graben along the southern foothills of Bogda Mountains (Fig. 1b; Chen et al., 1985; Liao et al., 1987; XBGMR, 1993; Carroll et al., 1995; Yang, 2008; Yang et al., 2010), and also revealed from sections and wells in Fukang Sag and Jimsar Sag along the northern foothills of Bogda Mountains (Wang et al., 2018; Liu et al., 2022).

Recent paleotectonic and paleogeographic reconstruction places the Bogda Mountains at the southeastern Kazakhstan Plate, NE Pangea (Fig. 1c; modified from Scotese, 2014). The Bogda Mountains have been placed in a humid climatic belt during Permian, according to plate tectonic reconstruction and modern climatic zonation (Chumakov and Zharkov, 2003; Thomas et al., 2011; Obrist-Farner and Yang, 2016). Petrographic and geochemical evidences suggest the Lucaogou Formation was deposited under dominantly semiarid climate, with less arid climate in the southern Bogda Mountains (Yang et al., 2010) and more arid climate in the northern Bogda Mountains (Liu et al., 2022).

The Lucaogou Formation is overlying the upper Daheyan Formation and beneath the Hongyanchi Formation in the lower Permian (Fig. 2). The ages of the Lucaogou Formation are still in debated. We tentatively access the Lucaogou Formation as Sakmarian deposits, as poorly constrained by U/Pb zircon ages (Fig. 2; Yang et al., 2010, 2013; Obrist-Farner and Yang, 2016; Tang et al., 2022), with lithostratigraphic, biostratigraphic, and chemostratigraphic constrains (Zhan, 2019; Wu et al., 2021). The Lucaogou Formation, as typical fluctuating-profundal facies association, consists of dominantly well-laminated black shales, dark gray mudstones, gray to grayish green dolomitic mudstones, wave-rippled siltstones, and fine-grained sandstones in the southern Junggar Basin (Carroll, 1998; Bohacs et al., 2000). The Lucaogou lacustrine high-order cycles in the study area mainly contain fluvial-lacustrine siliciclastics, carbonates, and paleosols and are at a scale of 0.1–1 m thick, reflecting systematic changes of stream, lake-plain, littoral, to profundal environments during lake contraction and expansion (Yang et al., 2010). High-frequent fluctuations of lake depth and depositional environments suggest that the Lucaogou lake was mainly a balance-filled lake basin, driven by paleoclimate variation between subhumid to semiarid (Carroll, 1998; Bohacs et al., 2000; Yang et al., 2010; Liu et al., 2022). The Lucaogou meter-scale cycles are sedimentary cycles, as repetitive vertical stacking of depositional systems that were resulted from repetitive lateral environmental shifts in stratigraphic records at a locality, reflecting repetitive environmental shifts and associated changes in environmental conditions and sedimentary processes (Yang et al., 2010). A depositional system consists of lithofacies that are linked by sedimentary processes within a depositional environment (Brown et al., 1977). A succession of the high-order cycles with an upward trend of deepening and shallowing of depositional environments is similar to a depositional sequence and associated systems tracts as defined in marine settings (Mitchum et al., 1991; Yang et al., 2010).

3. Samples and methods

Fifteen samples of siltstone, sandstone, black shale, dolomitic shale, calcareous shale, wackestone, and dolostone have been collected in four fluctuating profundal high-order cycles at a meter-scale in the north Tarlong section for petrographic observations and geochemical analyses. Care has been taken to select samples that are at least 30 cm beneath surface and have no signs of surface weathering (Yang et al., 2010).

Petrographic studies have been used to identify lithofacies and interpret depositional environments, including field investigations and microscopic observations on composition, sedimentary texture and structure, and fossils on hand samples and thin-sections, with reference to the stratal geometry and boundary relationship. Mineral composition analysis was conducted using an x-ray diffractometer (XRD Model: Olympus Innova-X BTX-II), equipped with a Co radiation source and operated at 31 kV and 0.4 mA. The exposure time was 70 min, with an exposure rate of 3 times/min. Scanning measurements of powered samples were performed in the range of 3°–55° (2θ), with a scanning speed of 0.02° (2θ)/min. Results of relative mineral compositions were estimated semiquantitatively, using peak area of major minerals and normalized to a total of 100%.

All geochemical analyses were performed in State Key Laboratory of Organic Geochemistry, Guangzhou Institute of Geochemistry, Chinese Academy of Sciences. Samples were first decontaminated through sonication in deionized water and then oven-dried at 40 °C. Samples were then crushed to a 100-mesh size (<0.15 mm) before use for all the geochemical analyses.

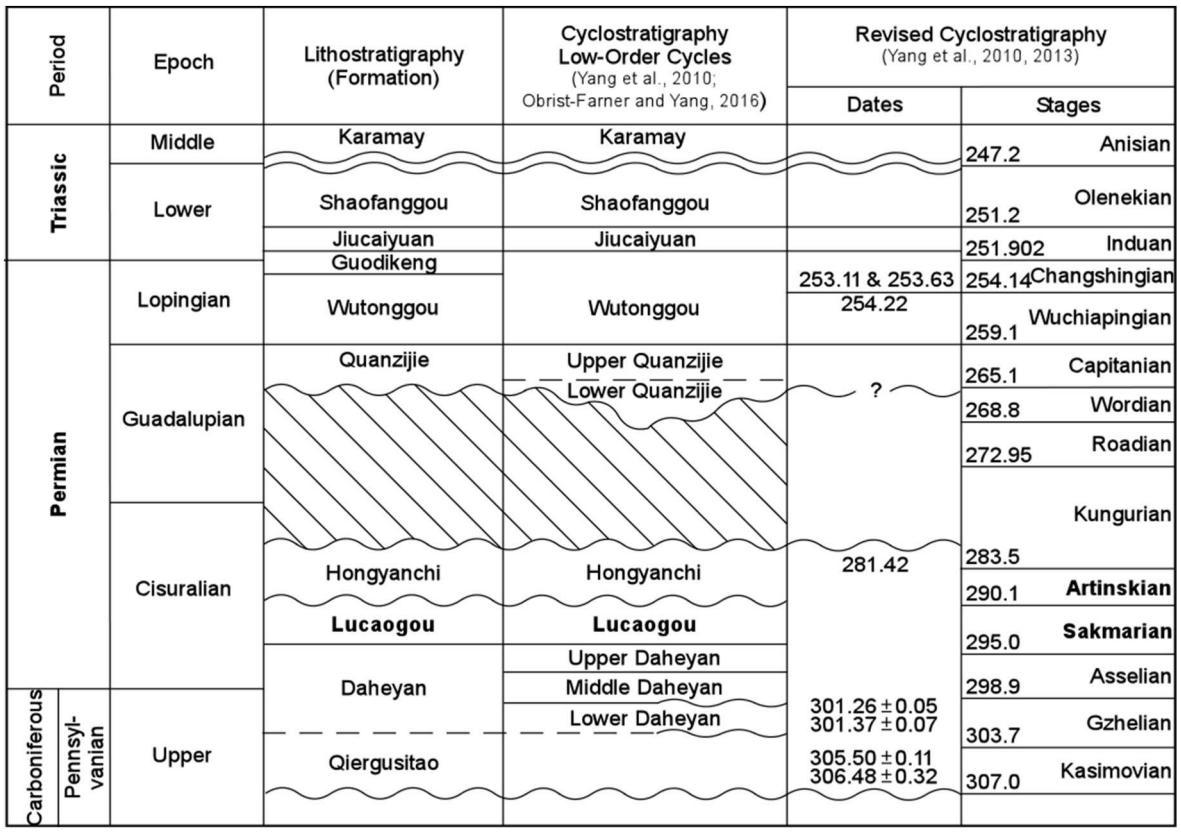

Fig. 2. Chrono-, litho, and cyclostratigraphy of the Upper Carboniferous-Middle Triassic strata in the Tarlong-Taodonggou area. Hachured areas indicate missing strata; wavy lines are major unconformities; and dashed lines are disconformities; Absolute ages at stage boundaries are from Cohen et al. (2013). Modified from Yang et al. (2010, 2013) and Obrist-Farner and Yang (2016).

Calcite equivalent content ($CaCO_3$ %) has been measured from inorganic carbon concentration (CO_3^{2-}) for duplicated samples, under the assumption that CO_3^{2-} is present as $CaCO_3$. $CaCO_3$ (%) was calculated using a carbonate content analyzer (Model: GMY-3). Volume of CO_2 was measured after 200 mg samples have completely reacted with sufficient amounts of hydrochloric acid (10 vol %). $CaCO_3$ (%) value of each sample was evaluated through comparing CO_2 values and that released from completed reaction of pure calcite and the acid. We recognize the inherent errors in this assumption (i.e. CO_3^{2-} is present as $CaMg(CO_3)^2$, and carbonates other than $CaCO_3$ are present). Nevertheless, the estimated $CaCO_3$ shows trend of calcareous minerals in accordance with calcite content measured from the XRD results.

Total organic carbon (TOC) content was measured with a Leco SC-632 carbon sulfur analyzer, through combustion of the organic carbon to CO_2. 10 mg crushed samples were soaked in a sufficient amount of hydrochloric acid (10 vol %) to remove carbonate. The samples were washed with deionized water until neutral and dried in the oven at 40 °C for 12 h before combustion. The combustion oven temperature was held at 400 °C for 3 min and heated to 850 °C for 5 min at a rate of 25 °C/min. Precision of duplicate samples is ±0.025‰, with detection limit of 0.2% for TOC.

Kerogen extraction started by pretreating ~20 g crushed samples with hydrochloric and hydrofluoric acid to remove all carbonate and siliciclastic components, respectively, following procedures of Durand and Nicaise (1980). Acid-insoluble residues were centrifuged and washed with deionized water until neutral. Proportions of carbon (C) and nitrogen (N) content in kerogen were measured using an Elemental Analyzer (Model: Vario Macro Cube, Elementar, Germany), via the combustion method after Prahl et al. (1980). Atomic carbon over nitrogen ratio (C/N) is calculated as C/N=(C/12)/(N/14). Stable organic isotopic composition ($\delta^{13}C_{org}$) was measured using combustion system, with a coupled elemental analyzer and isotope ratio mass spectrometer (Model: ThermoFinnigan Delta XL Plus GC-IRMS). Kerogen samples of 20–80 μg were added to a stannum boat and combusted at 1800 °C under helium carrier gas, following Craig (1953). Isotope ratios are determined based on delta notation (‰) relative to the Vienna Pee Dee Belemnite (V-PDB) standard after Craig (1957). Precision of duplicated samples is better than ±0.08‰ for the measurement of $\delta^{13}C_{org}$. Influence of in situ bitumens to the C/N ratio and $\delta^{13}C_{org}$ of kerogen is limited, as few bitumens exist within all the samples that are not mature.

Saturated fraction of dissolved organic matter has been used for biomarker analysis. Organic matter was first extracted from 100 g crushed samples, using a solvent mixture of dichloromethane and methanol at a 9:1 ratio at 48 °C for 72 h. Copper sheets were added in the Soxhlet apparatus to remove sulfur. After evaporative removal of extraction solvent, the extracts were dissolved in hexane and centrifuged to remove asphaltenes. Maltenes were fractionated by column chromatography, using activated thin layer of alumina and silica gel. Aliphatic, aromatic, and polar fractions were separated using hexane, a mixture of hexane and dichloromethane at a 3:2 ratio, and methanol, respectively.

The saturated fraction was analyzed using Agilent 7890A Gas Chromatography (GC) and Thermo Trace GC Ultra/DSQII Gas Chromatography-Mass Spectrometry (GC-MS), following the same heating procedure. GC was coupled with a 5975C MSD instrument and Triple-Axis Detector, using a HP-5 fused silica capillary column with a size of 30 m × 0.25 mm i.d. and 0.25 μm film thickness. Helium (400–700 kPa) was used as carrier gas, at a flow rate of 1.0 ml/min. Samples were injected in a splitless mode, with the injector and detector temperature at 290 °C and 300 °C, respectively. The oven temperature was set initially at 80 °C and held for 2 min, then increased to 300 °C at a heating rate of 4 °C/min and held for 25 min. The MS was operated in electron ionization (EI) mode at an energy of 70 eV. The MS full scan

ranged from m/z 50 to 600, with a 0.5 s total scan time. The selected ion monitoring (SIM) included following ions: $m/z = 125, 191, 217, 314$ for the saturated fraction. Interpretation of GC and GC-MS data was done using Chemstation software and Xcalibur software, respectively. Identification of individual compounds was achieved by comparing mass spectra and fragmentation patterns with literature and library data, authentic standards, and published mass spectra (Peters et al., 2005).

4. Results

4.1. Lithofacies

The four fluctuating profundal high-order cycles in the north Tarlong section are 1 m thick and consist of similar lithofacies associations in each cycle. Four types of lithofacies have been identified in the four high-order cycles, including interbedded and interlaminated coarse siltstone and very fine sandstone, black shale, dolomitic and calcareous shales, and wackestone and dolostone (Fig. 3a and b). They have distinct mineral composition, sedimentary texture and structure, fossil, and/or stratal geometry (Table 1; Fig. 4).

4.1.1. Lithofacies-I: interbedded and interlaminated coarse siltstone and very fine sandstone

Coarse siltstone and very fine sandstone are commonly interbedded and interlaminated. Sandstones are greenish gray to blackish gray and occur in beds of 2–20 cm thick (Fig. 3a–c). The framework grains are mainly in very fine sand size, a few others are silt size and medium to coarse sand size (Fig. 5a). Fine-sand grains are composed of monocrystalline quartz. Randomly scattered medium- and coarse-sand grains are mud clasts. Silt-size grains are principally quartz and plagioclase or K-feldspar, with minor lithic, heavy minerals (e.g., magnetite), and light minerals (e.g., micas). Most plagiclase have been partially altered to sericite. Matrix is ~5% and exclusively composed of clay minerals. Cement is composed of calcite and dolomite. The compositions of lithic

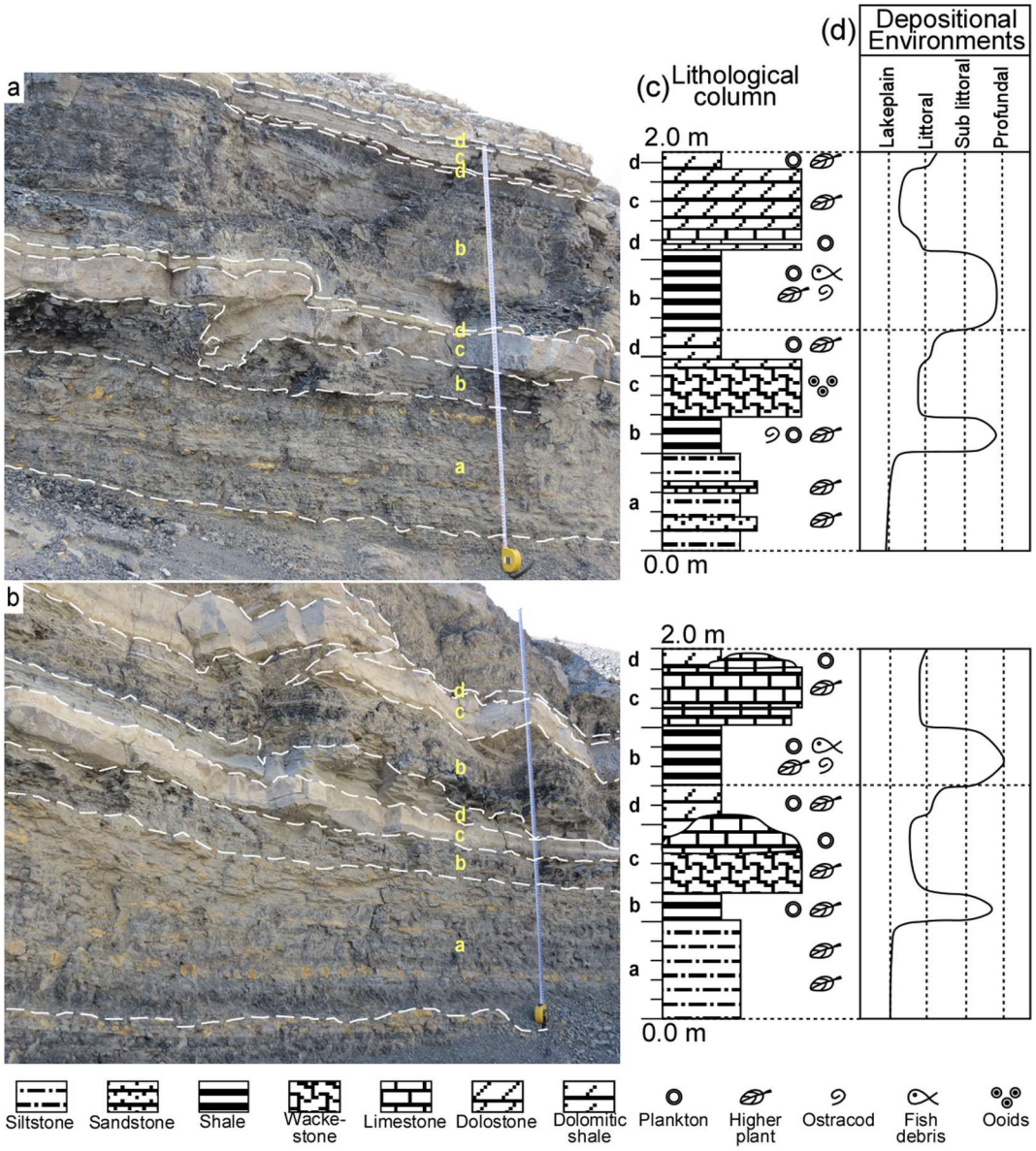

Fig. 3. (a–b) Outcrop photography of the Lucaogou lacustrine deposits, showing 4 m-scale high-order cycles. Four lithofacies have been identified in the four high-order cycles, including a: interbedded and interlaminated coarse siltstone and very fine sandstone; b: black shale; c: wackestone and dolostone; and d: dolomitic and calcareous shales. (c) Lithological columns of the four high-order cycles, showing distinctive lithologies, sedimentary texture and structure, fossil, and/or stratal geometry of the four lithofacies. (d) Depositional environments of individual lithofacies, showing cyclic changes of depositional environments from littoral to profundal during lake contraction and expansion.

Table 1
XRD results of mineral composition of four lithofacies in the high-order cycles.

Sample No.	Quartz	Feldspar (Na)	Feldspar (K)	Calcite	Dolomite	Kaolinite	Magnetite	Titanomagnetite	Zeolite
Lithofacies-I: Interbedded and interlaminated coarse siltstone and very fine sandstone									
XZ15-1	31.9	26.0	0.0	9.1	4.1	14.2	9.1	3.5	2.1
XZ15-9	30.0	0.0	28.9	9.2	3.9	14.1	8.6	3.3	2.2
Lithofacies-II: Black shales									
XZ15-6	41.7	15.7	0.0	14.6	4.3	12.1	7.3	2.4	1.8
XZ15-5	41.1	15.9	0.0	8.5	5.3	15.8	7.8	2.7	2.9
XZ15-2	52.1	17.2	0.0	15.0	4.0	0.0	7.5	2.9	1.3
XZ15-13	30.6	19.9	0.0	4.3	22.1	11.7	7.1	2.4	1.9
XZ15-10	41.8	16.8	0.0	7.1	8.6	14.7	6.8	2.1	2.1
Lithofacies-III: Wackestone and dolostone									
XZ15-7	24.8	14.4	0.0	4.2	37.0	10.6	7.8	0.0	1.3
XZ15-3	27.7	0.0	0.0	72.3	0.0	0.0	0.0	0.0	0.0
XZ15-15	45.5	0.0	0.0	7.8	36.4	0.0	6.2	2.5	1.6
XZ15-14	24.1	0.0	0.0	33.1	27.7	0.0	8.6	3.6	2.9
XZ15-11	31.8	0.0	0.0	44.6	7.5	0.0	12.2	3.9	0.0
Lithofacies-IV: Dolomitic and calcareous shales									
XZ15-8	47.5	0.0	0.0	3.7	26.6	11.2	7.1	2.4	1.5
XZ15-4	34.6	22.2	0.0	3.8	26.9	0.0	8.0	3.0	1.6
XZ15-12	24.2	19.3	0.0	19.1	13.7	12.4	7.2	2.4	1.6

Mineral composition (%) is calculated as the content of each mineral over all minerals.

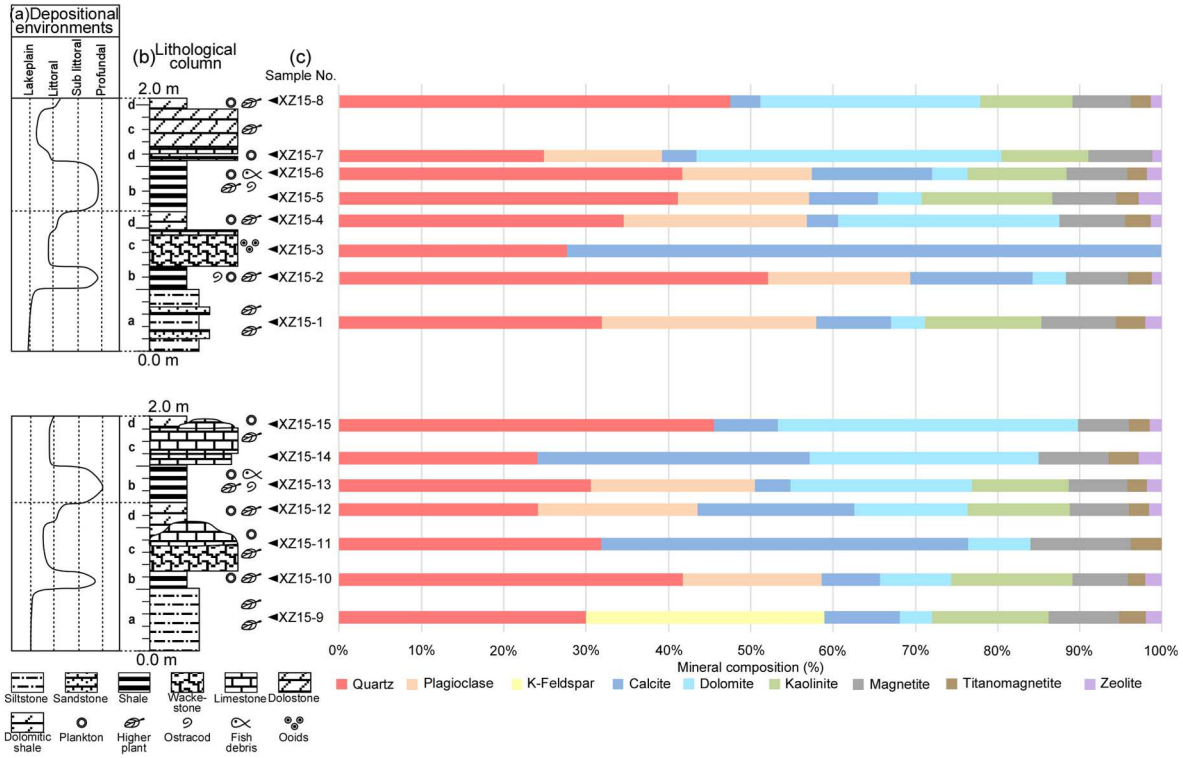

Fig. 4. (a) Depositional environments and (b) lithological columns of the four high-order cycles. (c) x-ray diffractometer (XRD) results of fifteen samples from the four high-order cycles. Results of relative mineral compositions were estimated semiquantitatively, using peak area of major minerals and normalized to a total of 100%.

grains are unidentified due to their small size. The results of mineral compositions described based on microscopic observations are also supported by the XRD results of sample XZ15-9 in Lithofacies-I (Table 1; Fig. 4). The sandstone is classified as very fine arkosic arenite. The sandstones are poorly sorted and angular to sub-rounded. Parallel and wavy laminations are continuous and moderately developed, with lamina usually ≤1 mm (Fig. 5a and b). Mud clasts are angular to sub-angular and well imbricated (Fig. 5b). Abundant plant remains and woody debris are in coarse-silt to coarse-sand size and usually imbricated along bedding plane, whereas sparse amorphous organic matter is present in the mud clasts or randomly scattered (Fig. 5c). Phytoclasts are commonly opaque, angular lath-shaped, with sharp distinct edges. The internal structure of the phytoclasts is usually infilled and obliterated, result in massive and invisible biostructure. Amorphous organic matter is reddish brown to dark black, diffuse-edged, irregular-shaped, and structureless. A rare skeletal fragment has zooecial walls with rounded pores (Fig. 5d). The walls are aragonitic, while the pores are filled with organic matter. It is possibly a bryozoan fossil.

Coarse siltstone is brownish gray to reddish brown and in beds 20–40 cm (Fig. 3–c). It contains sandy and gravel grains in the lower part and it is upward-fining and thinning. Sand to granule-size grains are dominantly paleosol clasts. Silt grains are mainly quartz and K-feldspar,

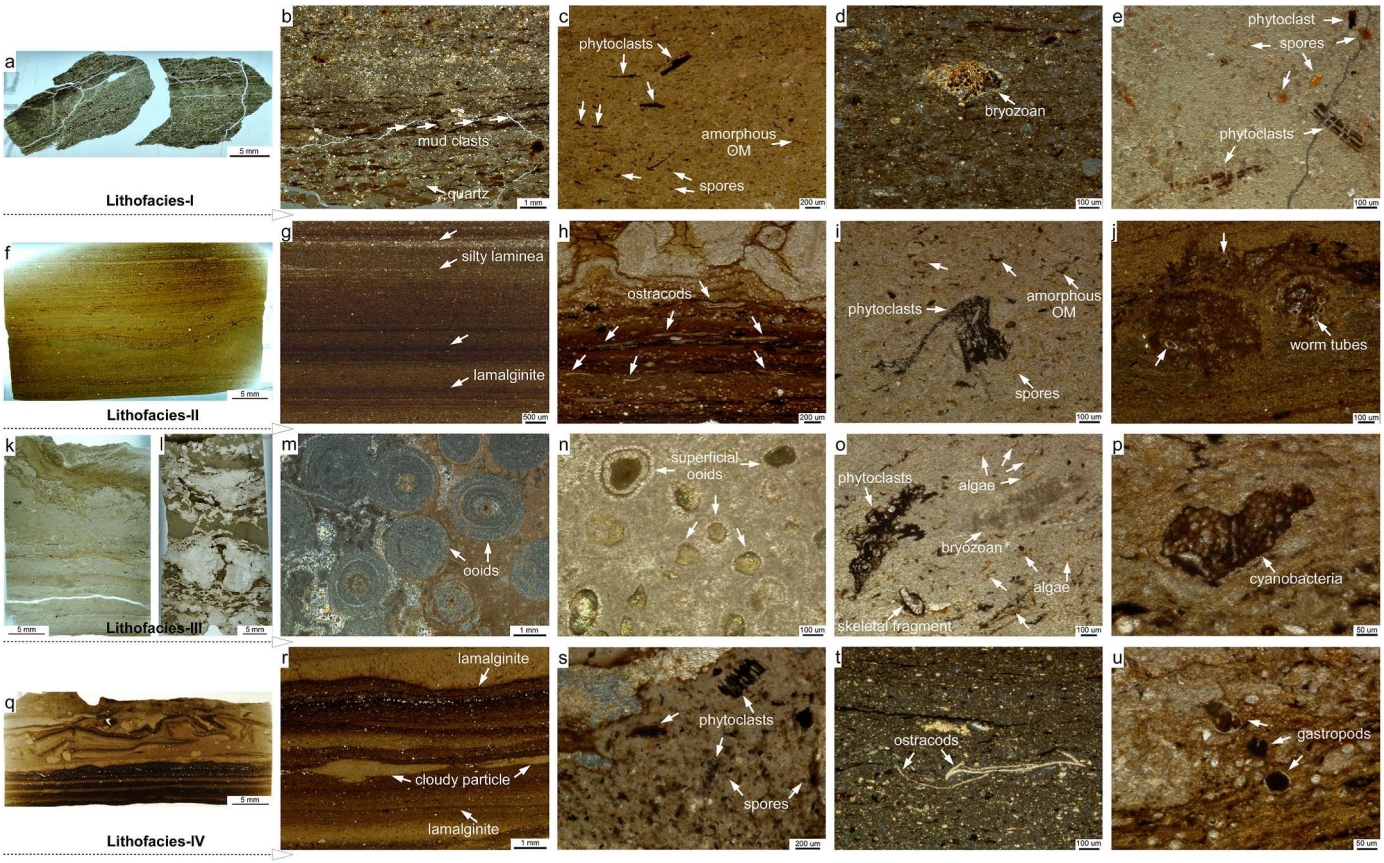

Fig. 5. Photomicrographs of four lithofacies: (a–e) Lithofacies-I: interbedded and interlaminated coarse siltstones and very fine sandstones; (f–j) Lithofacies-II: black shales; (k–p) Lithofacies-III: wackestones and dolostones; (q–u) Lithofacies-IV: dolomitic and calcareous shales. (a) A very fine sandstone sample (XZ15-1), it is weakly laminated and contains abundant plants remain. (b) Siliciclastic laminae of very fine sandstone in (a), showing framework grains of quartz and well imbricated mud clasts. (c) Phytoclasts, spores, and amorphous organic matter in a very fine sandstone sample; phytoclasts are opaque, elongate, and angular; spores are orange to reddish brown; amorphous organic matter is reddish brown and irregular-shaped. (d) A bryozoan fragment in a very fine sandstone sample; a transverse section of the skeletal fragment in a single grain shows zooecial walls and rounded pores, with organic matter filling inside the pores. (e) Phytoclasts and spores in a coarse siltstone sample (XZ15-9); the opaque biostructured phytoclasts break up into lath-shaped particles by splitting along the grain, noting splintery nature and brittle character; the angular outline, elongated shape, and structural grains are clear evidence of phytoclast structure; the orange fragments may be spores of uncertain affinity. (f) A black shale sample (XZ15-10), showing organic-rich, very well parallel, and algal laminae, with local erosional surfaces in the lower part; it contains abundant ostracods, fish scales and skeletons; it is interpreted as dysoxic profundal deposits. (g) A black shale sample (XZ15-5), showing silty laminae and lamalginite. (h) Highly compressed ostracodes in a black shale sample; they consist of single and a pair of ostracode valves with carapace interior, aligned parallel to the organic-rich laminae. (i) A black shale sample, showing opaque phytoclasts with internal lath-shaped structure. (j) Worm tubes in a black shale sample; a transverse section of a bundle of worm tubes in a single grain, with organic matter filling inside the tubes. (k) A wackestone sample (XZ15-14), the lower part is parallel laminated and rich in siliciclastics and organics; the upper part is wrinkly parallel laminated. (l) A dolostone sample (XZ15-7), it is parallel or wrinkly parallel laminated. (m) Concentrically coated ooids in a wackestone sample (XZ15-3), showing the peloidal nucleus and multiple concentric layers representing coatings of varied thickness. (n) Superficial ooids in a wackestone sample; they contain only one thin cortical coating of the detrital grain nuclei, isopachous calcite cement with radial structure in the cortex of the superficial ooids, and other detrital grains without coating. (o) Phytoclast, algae, bryozoan, and skeletal fragment in a limestone/wackestone sample (XZ15-11); phytoclast is similar to that in (i); amorphous organic matter is orange to transparent, irregular-shaped, and well preserved; it was most likely derived from algae; bryozoan has thin zooecial walls with rounded pores; origin of the skeletal fragment at the comer is unknown. (p) Cyanobacteria in wackestone; noting small 'bunches' in irregularly shaped clumps in transverse section are well preserved. (q) A dolomitic shale sample (XZ15-12), the lower part is parallel laminated and composed of couplets of organic-rich and dolomitic lamina; the upper part has a mixed layer characterized by wrinkly laminae, micro faults, mud cracks, and sand-size mud clasts. (r) Lamalginite and cloudy particles in a dolomitic shale sample (XZ15-12). (s) Phytoclasts and spores in a dolomitic shale sample; clear scalariform pitting in the opaque biostructured phytoclasts shows that the particle is derived from tracheid tissue, and the fine preservation of the microstructure suggests a charcoal origin. (t) Ostracodes in a dolomitic shale sample; A pair fish-hook-like terminations of a single ostracode valve, these terminations are distinctive features of identification of ostracode remains, in combination with carapace size, structure, and wall morphology. (u) Gastropod in a dolomitic shale sample; noting the outline of baby-bottom structure preserved by internal organic matter and external sediments in transverse section; The circular grain without chambers is pteropod.

with minor calcite and dolomite. Clay-size grains are mainly clay minerals. The mineral composition is constant with the XRD results of sample XZ15-9 in Lithofacies-I (Table 1; Fig. 4). Silts are equant, sub-angular to rounded and moderately sorted, whereas sands and granules are sub-angular to sub-rounded and poorly sorted. Abundant phytoclasts are mm-cm in size, well preserved, and randomly distributed (Fig. 5e). They are opaque, elongate, and lath-shaped, with angular and sharp external edges and internal scalariform pitting or cross-field pitting. Reddish orange spores are randomly scattered and commonly occur with phytoclasts (Fig. 5e).

4.1.2. *Lithofacies-II: Black shale*

Black shale is blackish gray to dark black, and occurs as 10–40 cm thick (Fig. 3a–c). It is composed of dominantly detrital grains and abundant organic matter (Fig. 5f). Detrital grains are mainly in clay to fine-medium-silt size, with rare coarse-silt size to fine granule size.

Discrete fine silts can be clearly seen without overgrowth under higher magnification observation (Fig. 5g and h). The silt-size grain are mainly quartz and plagioclase feldspar, while the sand-size grains are predominantly lithic fragments that were possibly from igneous and metamorphic rocks. Matrix mainly consists of calcite, dolomite, clay minerals, and other minerals, including magnetite, titanomagnetite, zeolite, and muscovite (Table 1; Fig. 4). Rare mud clasts range from coarse silt to fine granule size and commonly contain amorphous organic matter. The mud clasts commonly distort the underlying laminae and are overlain by continuous laminae. Black shale is dominantly mm-to-sub-mm well-parallel laminated, with both silty laminae and lamalginite (Fig. 5f and g). The laminae are generally continuous, and in some case, wavy and climbing rippled (Fig. 5f). The bedding plane is sharp to gradational and, in places, rarely erosional. This lithofacies is principally organic-rich, and variably calcareous or dolomitic (Table 1; Fig. 4). It contains common plant remains, amorphous organic matter, intact ostracod, and sparse fish scales, spores, and other skeletal fragments. Ostracods have distinctive features of a pair fish-hook-like terminations of single and articulated valves, with carapace interior and wall morphology (Fig. 5h). They are highly compressed and aligned parallel to the organic-rich laminae. Abundant phytoclasts are opaque, angular, elongate, and contain internal lath-shaped structure (Fig. 5i). Reddish orange spores commonly occur with phytoclasts and are locally concentrated on bedding plane (Fig. 5i). Amorphous organic matter is reddish brown to black, diffuse-edged, structureless (Fig. 5i), and abundant in the lamalginite (Fig. 5g). Some fine-sand-sized clasts have irregular shape and contain various tubes inside (Fig. 5j). These tubes have siliciclastic walls and they are filled with organic matter. They are probably worm tubes.

4.1.3. Lithofacies-III: Wackestone and dolostone

Wackestone is gray to dark gray, well-bedded and laterally consistent, in beds 10–40 cm (Fig. 3a–c). The lower part of wackestone is parallel laminated and rich in siliciclastics and organics; the upper part is wrinkly parallel and micritic (Fig. 5k). Wackestone lithofacies commonly contains detrital quartz, feldspar, lithic grains, and allochems, with calcareous and dolomitic matrix and cement (Table 1; Fig. 4). Detrital grains are mainly medium-coarse silt-sized and angular to sub-angular. Allochems include skeletal fragments, ooids, superficial ooids, pellets, and intraclasts. Skeletal fragments are mainly bivalves, gastropods, ostracods, bryozoan, fish bones, fish scales, and some unidentified skeleton grains. Well-preserved bivalves and fish skeletons are locally abundant. Ooids range from coarse silt to coarse sand in size and have peloidal nuclei and multiple radial and concentric cortices (Fig. 5m). Superficial ooids are mainly coarse silt to very fine sand-sized, with a thin cortex on irregular and angular lithic nuclei (Fig. 5n). Isopachous calcite cement with radial structure are commonly in the cortex of the superficial ooids. Intraclasts and pellets are commonly blackened, micritic, and in silt to pebble size. Intraclasts are mostly micritic; some are grapestones. Common algae occur as reddish brown stains or asphalt along the wrinkly parallel laminae (Fig. 5k–o). Rare lumps containing apparent cell structures are present in wrinkly parallel laminae. Common opaque phytoclasts are in fine to very coarse sand-size. The phytoclasts have elongate sharp outlines and scalariform pitting (Fig. 5o). Bryozoan has thin zooecial walls with rounded pores (Fig. 5o). Sparse possible cyanobacteria have various well preserved small bunches in irregularly shaped clumps (Fig. 5p).

Dolostone is yellowish gray to dark brown and dense, and occurs as 1–20 cm thick (Fig. 3a–c). It reacts slowly with dilute hydrochloric acid. It is mainly composed of dolomitic mud or microspars and siliciclastic mud of quartz. This dolostone contains dolomite and dolomitic limestone, with pure dolomite laminae and dolomitic shale laminae (Fig. 5l). Skeletal grains and organic matter in dolostone are similar to those in the wackestone.

4.1.4. Lithofacies-IV: Dolomitic and calcareous shales

Dolomitic and calcareous shales are yellowish brown, gray to dark gray, and black, and in beds 10–20 cm (Fig. 3a–c). They are mainly composed of quartz, feldspar, clay minerals, dolomite or calcite, and a few lithic fragments. This is also supported by mineral composition from the XRD results (Table 1; Fig. 4). Quartz and feldspar dominate and are in fine-medium silt size. The content of dolomite and calcite varies. Dolomite and calcite are microcrystalline. Rare elongate gypsum crystals and sand-size calcified nodules are present in some other similar samples (Yang et al., 2007, 2010).

Dolomitic and calcareous shales are interlaminated at a sub-mm to mm scale (Fig. 5q and r). The laminae are dominantly parallel, sometime wrinkly, and rarely lenticular (Fig. 5q and r). The parallel laminae are composed of couplets of organic-rich and dolomitic/calcareous lamina (Fig. 5q). They are overlain by a mixed layer characterized by wrinkly laminae, micro faults, mud cracks, and sand-size mud clasts. The contact is erosional. Sparse mud clasts range from coarse silt to coarse sand size, sub-angular to rounded. A few of them distorted the underlying laminae and are covered by continuous laminae. Amorphous organic matter is abundant in lamalginite; phytoclasts and ostracods are common and concentrated along beddings, whereas fish scales and skeletons are sparsely scattered. Amorphous organic matter is reddish brown to black, irregular-shaped, and structureless. It is generally concentrated in laminae to form lamalgnite, especially, it is highly abundant and randomly distributed in the overlain wrinkly laminae (Fig. 5q and r). Some of the amorphous organic matter is in granule size. Some of the sand-size grains are rounded, with smooth and organic wall, and thus likely algae. Phytoclasts are opaque, elongate, angular, and locally concentrated in parallel laminae. They have sharp edges and internal scalariform pitting or cross-field pitting (Fig. 5s). Reddish orange spores are randomly scattered and commonly occur with phytoclasts (Fig. 5s). Gastropods and ostracods are well preserved and range from medium to coarse silt in size and coarse silt to coarse sand in size, respectively (Fig. 5t and u). Common ostracodes have a pair fish-hook-like terminations and distinctive wall morphology and structure (Fig. 5t). Gastropods are characterized by outline of baby-bottom structure preserved by internal organic matter and external sediments in transverse section (Fig. 5u).

4.2. Organofacies

Four distinctive organofacies have been identified in the four high-order cycles, on the basis of specific bulk geochemical parameters related to abundance and geochemical composition of organic matter and specific biomarker proxies related to organic matter type, instead of other proxies related to depositional condition and thermal maturity (Table 2). These bulk geochemical parameters include total organic carbon (TOC) content, atomic ratio of hydrogen over carbon (H/C) and carbon over nitrogen (C/N), and organic carbon isotopic composition ($\delta^{13}C_{org}$; Tables 2 and 3). These biomarker proxies include proposition of short-chain (C_{12}–C_{19}), mid-chain (C_{20}–C_{25}), and long-chain *n*-alkanes (C_{26}–C_{34}), terrestrial over aquatic ratio (TAR), and 17α-hopanes over regular $C_{27\text{-}29}$ steranes ratio (hopane/sterane; Tables 2 and 3).

4.2.1. Organofacies-I

Organofacies-I 1 is characterized by TOC contents of 0.2–0.3 wt%, H/C ratios of 1.65–1.74, C/N ratios of 25.9–26.3, and $\delta^{13}C_{org}$ values of −22.5 to −21.8 ‰ (Table 2; Fig. 6c–f). Organofacies-I is also marked by *n*-alkanes of long-chain ($C_{26–34}$) ≥ mid-chain ($C_{20–25}$) > short-chain ($C_{12–19}$), TAR of 0.6–2.5, regular steranes $C_{29} > C_{28} > C_{27}$ with mean proportions of 42%: 32%: 26%, and sterane/hopane ratios of 1.9–2.4 (Table 2; Fig. 7a–d).

4.2.2. Oragnofacies-II

Oragnofacies-II is distinguished by TOC contents of 2.8–4.8 wt%, H/C ratios of 1.63–1.94, C/N ratios of 40.0–47.8, and $\delta^{13}C_{org}$ values of

Table 2
Selected organic geochemical attributes of organofacies.

Sample No.	TOC (wt.%)[a]	$CaCO_3$ (%)[b]	H/C[c]	C/N[d]	$\delta^{13}C_{org}$ (‰)[e]	Peak[f]	CPI[g]	OEP[h]	N-alkanes (%)[i]			TAR[j]	Pr/Ph[k]	β-carotane[l]	Ga. Index[m]	Homohop. Index[n]	Hop./Ste.[o]	Regular Ste. (%)[p]			Diast. Index[q]	Ts/(Ts + Tm)[r]	C_{30}hop βα/(βα+αβ)[s]	C_{29} S (S+R)[t]	C_{29} αα/(αα +ββ)[u]
									S	M	L							C_{27}	C_{28}	C_{29}					
Organofacies-I																									
XZ15-1	0.34	7.9	1.74	25.9	−21.8	C_{16}	1.5	1.4	34	36	30	0.67	1.38	n. d.	0.0	0.0	1.9	37	30	33	0.18	0.38	0.12	0.36	0.51
XZ15-9	0.25	14.5	1.65	26.3	−22.5	C_{29}	2.1	1.6	20	24	56	2.51	1.25	n. d.	0.0	0.0	2.4	27	22	51	0.12	0.22	0.28	0.49	0.36
Organofacies-II																									
XZ15-6	3.12	15.1	1.87	46.3	−26.1	C_{21}	1.2	1.2	50	37	13	0.17	1.45	trace	1.48	0.32	2.8	39	32	29	0.13	0.60	0.09	0.53	0.41
XZ15-5	2.92	13.3	1.66	43.3	−24.8	C_{21}	1.3	1.4	40	38	22	0.39	1.57	n. d.	0.96	0.49	1.3	38	35	27	0.09	0.45	0.15	0.57	0.35
XZ15-2	3.45	22.4	1.63	46.5	−24.1	C_{20}	1.4	1.3	43	40	17	0.24	1.45	n. d.	1.48	0.09	4.8	33	33	34	0.15	0.64	0.13	0.53	0.43
XZ15-13	4.77	37.3	1.94	40.0	−25.3	C_{25}	1.4	1.3	25	36	39	1.08	1.58	trace	2.17	0.46	2.5	45	29	26	0.18	0.59	0.12	0.38	0.30
XZ15-10	2.81	16.8	1.86	47.8	−26.2	C_{20}	1.3	1.2	42	40	18	0.30	1.45	n. d.	1.39	0.48	4.5	32	35	33	0.17	0.70	0.06	0.53	0.43
Organofacies-III																									
XZ15-7	1.31	72.0	1.76	42.5	−25.7	C_{21}	1.3	1.3	29	43	28	0.59	1.47	trace	1.34	0.23	2.8	42	34	24	0.12	0.63	0.11	0.40	0.47
XZ15-3	0.74	97.0	1.67	39.5	−25.5	C_{21}	1.4	1.3	33	48	19	0.31	1.61	n. d.	1.42	n. d.	3.8	37	30	33	0.15	0.61	0.14	0.55	0.43
XZ15-15	3.01	64.5	1.91	48.7	−27.2	C_{21}	1.3	1.3	32	39	29	0.57	1.44	trace	1.35	0.22	5.0	30	34	36	0.14	0.67	0.10	0.48	0.41
XZ15-14	0.89	96.3	1.91	42.2	−26.1	C_{23}	1.3	1.3	29	44	27	0.56	1.67	n. d.	1.36	n. d.	4.0	27	37	36	0.17	0.73	0.10	0.43	0.47
XZ15-11	1.49	83.3	1.61	42.7	−25.1	C_{23}	1.3	1.2	30	46	24	0.46	1.81	n. d.	1.25	n. d.	10.1	31	36	33	0.12	0.76	0.02	0.60	0.36
Organofacies-IV																									
XZ15-8	6.49	16.3	2.02	36.4	−28.6	C_{21}	1.4	1.3	42	44	14	0.19	1.88	n. d.	1.38	0.48	2.6	38	35	27	0.14	0.66	0.08	0.54	0.46
XZ15-4	6.11	18.7	1.89	49.9	−27.3	C_{21}	1.4	1.3	45	44	11	0.15	1.64	n. d.	1.75	n. d.	4.1	33	32	35	0.15	0.68	0.13	0.56	0.40
XZ15-12	5.85	51.3	2.14	46.6	−29.6	C_{21}	1.3	1.2	34	44	22	0.38	1.54	n. d.	1.54	0.31	4.7	26	42	32	0.16	0.69	0.07	0.53	0.44

Biomarker proxies: [a] total organic carbon content; [b] $CaCO_3$ (%) measured through reaction of sample with hydrochloric acid; [c] atomic hydrogen/carbon ratio; [d] atomic carbon/nitrogen ratio; [e] organic carbon isotope ratio (‰) relative to the V-PDB standard; [f] peak of *n*-alkanes in TIC traces chromatogram; [g-h] peak areas of *n*-alkanes in TIC traces chromatogram measured for calculating the CPI and OPE values: CPI = $[(nC_{25}+nC_{27}+nC_{29}+nC_{31})/(nC_{24}+nC_{26}+nC_{28}+nC_{30})+(nC_{25}+nC_{27}+nC_{29}+nC_{31})/(nC_{26}+nC_{28}+nC_{30}+nC_{32})]/2$; OEP=$(nC_{25}+6\times nC_{27}+nC_{29})/[4\times(nC_{26}+nC_{28})]$; [i] peak of *n*-alkanes in TIC traces chromatogram, S: short chain *n*-alkanes ($C_{12\text{-}19}$), M: mid-chain *n*-alkanes ($C_{20\text{-}24}$), and L: long chain *n*-alkanes ($C_{25\text{-}35}$) normalized to a total of 100%; [j] peak areas of *n*-alkanes in TIC traces chromatogram: TAR= $(nC_{27}+nC_{29}+nC_{31})/(nC_{15}+nC_{17}+nC_{19})$; [k] peak areas of isoprenoid in TIC traces from GC for acquiring pristane/phytane (Pr/Ph); [l] β-carotane in *m/z* 125 and 558 chromatogram, not determined (n. d.); [m] peak areas in *m/z* 191 chromatogram: gammacerane index (Ga. Index) = 10×gammacerane/(gammacerane + C_{30} 17α,21β-hopane); [n] homohopane index (Homohop. Index): peak areas of C_{35} 17α,21β,(22R + 22S)-pentakishomohopanes over peak areas of C_{33} counterparts in *m/z* 191 chromatogram; [o] 17α-hopanes/regular steranes (Hop./Ste.): peak areas of 17α,(22S + 22R)-hopanes consist of the $C_{29\text{-}33}$ pseudohomologs in *m/z* 191 over sum of 5α,14α,17α,(20R + 20S) and 5α,14β,17β,(20R + 20S) of C_{27} cholestanes, C_{28} methylcholestanes, and C_{29} ethylcholestanes in *m/z* 217 chromatogram; [p] peak areas of 5α,14α,17α,(20R + 20S) and 5α,14β,17β,(20R + 20S) of C_{27} cholestanes, C_{28} methylcholestanes, and C_{29} ethylcholestanes calculated in *m/z* 217 chromatogram and normalized to a total of 100%; [q] diasteranes index (Diast. Index): peak areas of C_{27} 13β,17α,(20R + 20S)-diacholestanes over sum of C_{27} 13β,17α,(20R + 20S)-diacholestanes, C_{27} 5α,14α,17α,(20R + 20S)-cholestanes, and C_{27} 5α,14β,17β,(20R + 20S)-cholestanes in *m/z* 217 chromatogram; [r] peak areas in *m/z* 191 chromatogram, Tm: 17α-22,29,30-trisnorhopane-C_{27}; Ts: 8α-22,29,30-trisnorneohopane-C_{27}; [s] peak area of C_{30} 17β,21α-moretane over sum of C_{30} 17β,21α-moretane and C_{30} 17α,21β-hopane in *m/z* 191 chromatogram; [t] peak areas of (ααα+αββ) 20S over sum of (ααα+αββ) 20S and (ααα+αββ) 20R of C_{29} ethylcholestanes in *m/z* 217 chromatogram; [u] peak areas of 5α,14α,17α,(20R + 20S) over sum of 5α,14α,17α,(20R + 20S) and 5α,14β,17β,(20R + 20S) of C_{29} ethylcholestanes in *m/z* 217 chromatogram.

Table 3
Selected geochemical proxies that are workable to identify organofacies.

Geochemical proxies	Proxy information	References
Total organic carbon (TOC)	Amount of residual organic matter in sedimentary rocks	Trask (1939); Tissot and Welte (1984); Meyers (2003)
Hydrogen/carbon ratio (H/C)	Types of kerogen	Tissot and Welte (1984)
Carbon/nitrogen ratio (C/N)	Proportions of algal and land-plant organic matter	Ishiwatari and Uzaki (1987); Jasper and Gagosian (1990); Prahl et al. (1994); Meyers (1997), 2003
Stable organic carbon isotope (δ^{13}Corg)	Origins of organic matter	Tissot and Welte (1984); Meyers (1997)
Long chain *n*-alkanes (nC_{26}-nC_{35})	Contributions of higher terrestrial plant waxes	Eglinton and Hamilton (1967); Rieley et al. (1991); Bush and McInerney (2013)
Intermediate chain *n*-alkanes (nC_{20}-nC_{25})	Contributions from aquatic macrophytes	Ficken et al. (2000); Sachsenhofer et al. (2006); Bush and McInerney (2013)
Short chain *n*-alkanes (nC_{12}-nC_{19})	Contribution of algae and microorganisms	Cranwell et al. (1987); Bush and McInerney (2013)
Terrestrial/aquatic ratio (TAR)	Proportions of organic matter from terrestrial plant over that from algae	Bourbonniere and Meyers (1996); Meyers (1997)
Regular steranes C_{27}, C_{28}, and C_{29}	C_{27} steranes derived from algae, phytoplankton and zooplankton; C_{29} steranes derived from vascular plants or specific freshwater microalgae	Rieley et al. (1991); Huang and Meinschein (1979); Volkman and Maxwell, 1986; Volkman et al., 1998, 2003, 2005;
17α-hopanes/ regular steranes ratio	Proportions of organic matter from prokaryotic organisms versus eukaryotic organisms	Moldowan et al. (1985); Peters et al. (2005); Horsfield et al., 1994

−26.2 to −24.1‰ (Table 2; Fig. 6c–f). It is also characterized by dominance of short-chain *n*-alkanes, TAR of 0.17–1.08, regular steranes $C_{27} > C_{28} > C_{29}$ with mean proportions of 37%: 33%: 30%, and hopane/sterane ratios of 1.3–4.8 (Table 2; Fig. 7a–d).

4.2.3. Organofacies-III

Organofacies-III is depicted by TOC contents of 0.7–3.0 wt%, H/C ratios of 1.61–1.91, C/N ratios of 39.5–48.7, and $\delta^{13}C_{org}$ values of −27.2 to −25.1‰ (Table 2; Fig. 6c–f). It is simultaneously outlined by dominance of mid-chain *n*-alkanes with a large number of short-chain *n*-alkanes, TAR of 0.31–0.59, regular steranes $C_{28} \geq C_{27} > C_{29}$ with mean proportions of 34%: 34%: 32%, and hopane/sterane ratios of 2.8–10.1 (Table 2; Fig. 7a–d).

4.2.4. Organofacies-IV

Organofacies-IV is characterized with TOC contents of 5.9–6.5 wt%, H/C ratios of 1.89–2.14, C/N ratios of 36.4–49.9, and $\delta^{13}C_{org}$ values of −29.6 to −27.3‰ (Table 2; Fig. 6c–f). Organofacies-IV is further portrayed by dominance of short-chain and mid-chain *n*-alkanes, TAR of 0.15–0.38, regular steranes $C_{28} > C_{27} \geq C_{29}$ with mean proportions of 36%: 32%: 32%, and hopane/sterane ratios of 2.6–4.7 (Table 2; Fig. 7a–d).

5. Discussion

5.1. Lithofacies and depositional environments

Four lithofacies can be classified by content of siliciclatic and carbonate minerals (i.e., quartz and feldspar v.s. calcite and dolomite; Fig. 6a), as well as organic carbon content and inorganic carbon content (i.e., TOC v.s. $CaCO_3$; Fig. 6b). The depositional environments of individual lithofacies were interpreted from composition, sedimentary texture and structure, fossils, boundary relationship, and facies associations (Fig. 3d). They were probably deposited in littoral to profundal

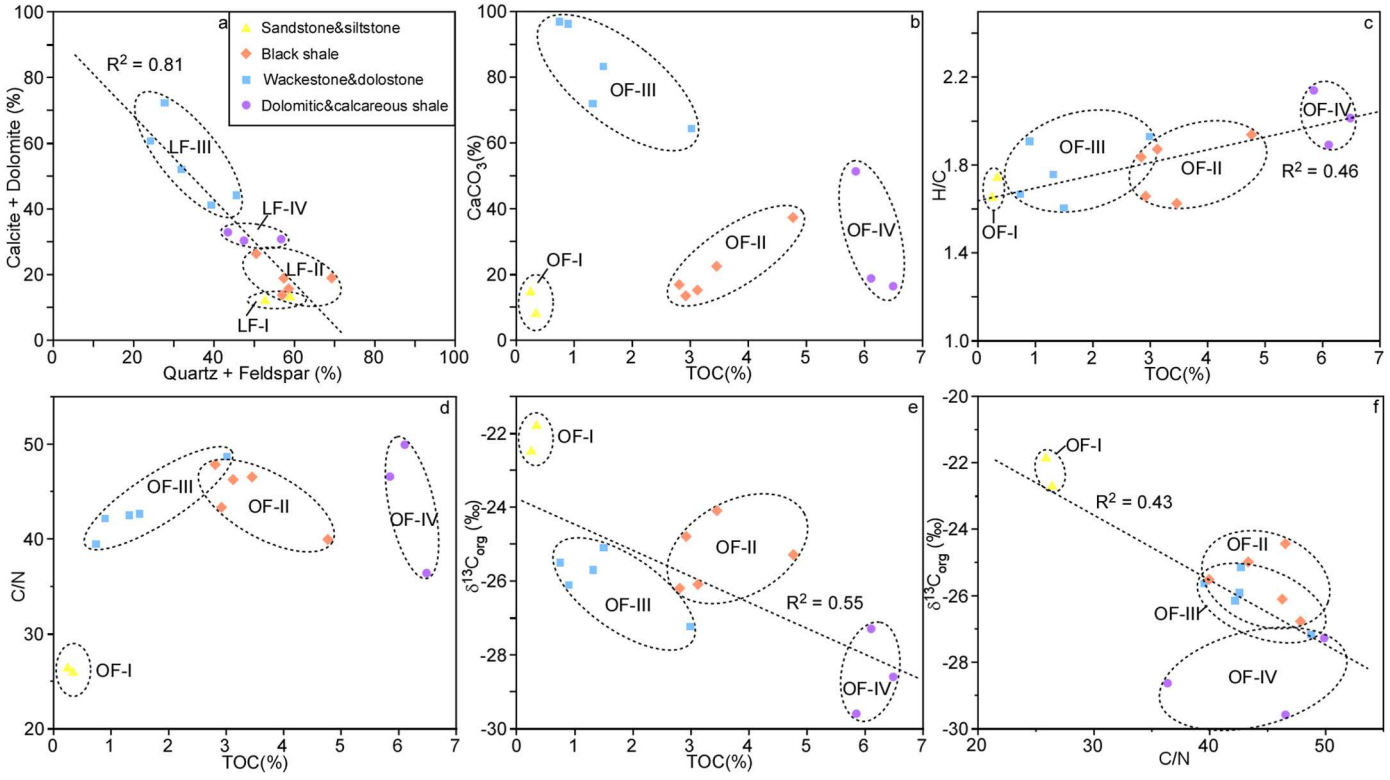

Fig. 6. Correlation between bulk organic geochemical proxies (a–d) and lithofacies with interpreted depositional environments. These proxies include (a) total organic carbon (TOC); (b) ratio of hydrogen over carbon (H/C); (c) ratio of carbon over nitrogen (C/N); (d) stable organic carbon isotope ratio ($\delta^{13}C_{org}$).

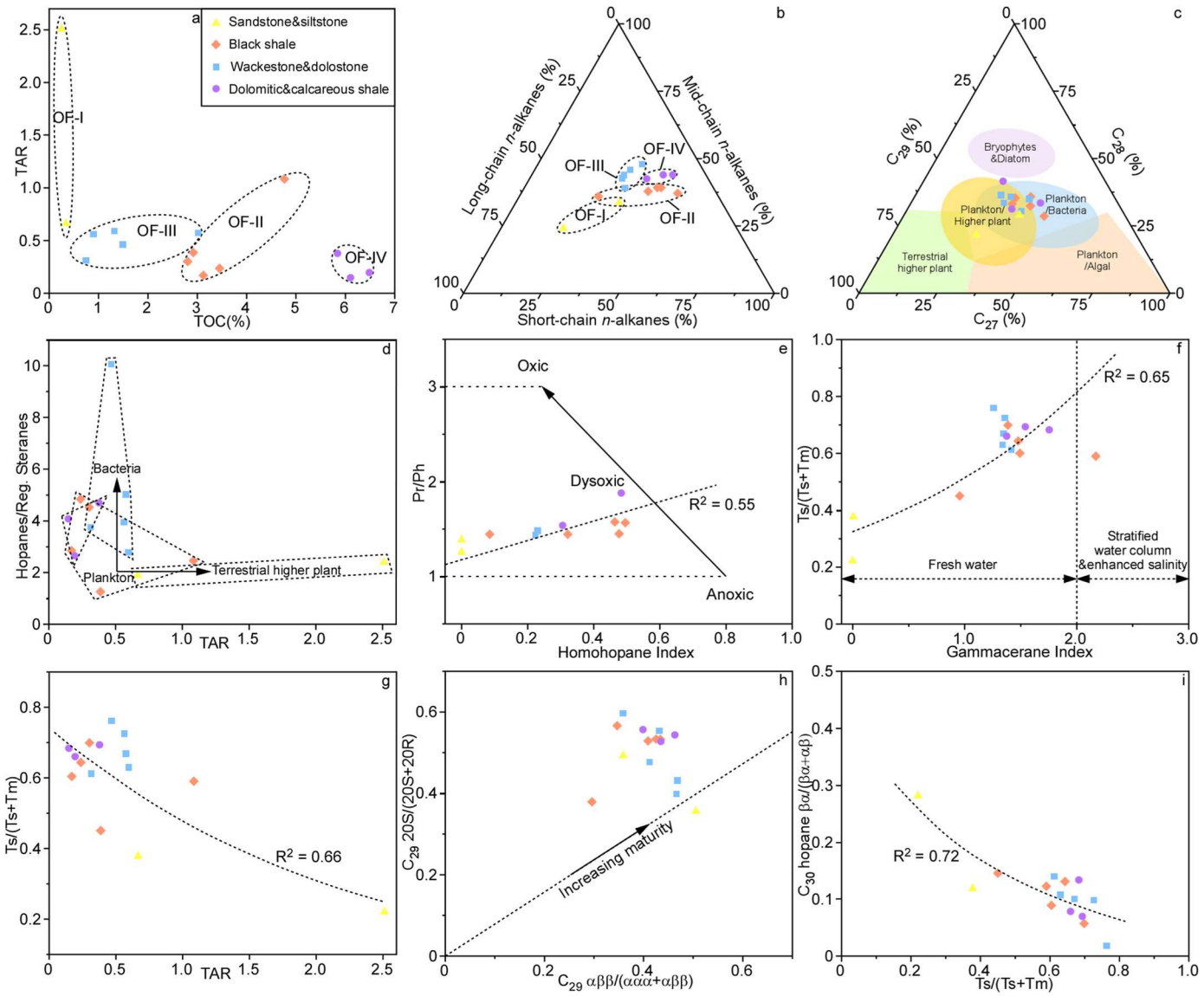

Fig. 7. Correlation between biomarker proxies (a–h) and lithofacies with interpreted depositional environments. Biomarkers related to organic matter types: (a) terrestrial aquatic ratio (TAR), TAR is calculated as ratio of *n*-alkanes of (C_{27}+C_{29}+C_{31})/(C_{15}+C_{17}+C_{19}); (b) proportions of short chain (C_{13}–C_{19}), intermediate-chain (C_{20}–C_{24}), and long-chain (C_{25}–C_{31}) *n*-alkanes; (c) proportions of C_{27} and C_{29} regular steranes; (d) regular steranes/17-a hopanes ratio. Biomarkers related to redox conditions: (e) pristane/phytane ratio (Pr/Ph) and (f) diasteranes index = C_{27} 13β(H),17α(H),(20R + 20S)-diacholestanes/C_{29} 5α(H),14α(H),17α(H),(20R + 20S)-24-ethylcholestanes. Biomarkers related to water column salinity: (g) gammacerane index = 10×gammacerane/(gammacerane + C_{30} 17α(H),21β(H)-hopane), and (h) Ts/(Ts + Tm) ratio (Ts = C_{27} 18α-trisnor-hopane Tm=C_{27} 17α-trisnor-hopane).

lacustrine environments during lake contraction and expansion. This is in accordance with the environmental interpretation from Yang et al. (2010, 2021) and in a highly fluctuating balance-filled lake (Carroll and Bohacs, 1999, 2001; Bohacs et al., 2000; Yang et al., 2010). Cyclic changes of depositional environments show systematic trends, suggesting high-order lacustrine expansion-contraction cycles (Fig. 3d).

The sandstones and siltstones are interbedded and interlaminated, and commonly overlie muddy paleosols of underlying cycle. They form an overall fining- and thinning-upward trend. The facies have a sharp to slightly erosional base and a gradational to sharp top. The mud clasts in sandstones are interpreted as paleosol rip-up clasts. Possible worm tubes suggest relatively oxic lake water condition. The lithofacies is interpreted as low-moderate energy lake-plain to littoral deposits during the earliest shoreline transgression (Fig. 3d), similar to interpretation from Yang et al. (2010).

Black shales commonly overlie interbedded and interlaminated siltstone and sandstone of Lithofacies-I, and underlie limestone of Lithofacies-III with gradational contacts. The mm-to-sub-mm laminae and absence of bioturbation suggest a low-energy, dysoxic to anoxic, profundal environment (Yang et al., 2007, 2010). The stratigraphic relationship with sub- and superjacent facies suggest they were probably deposited during the maximum transgression (Fig. 3d).

Wackestones commonly overlie black shales. High abundance of skeletal fragments indicates quiet and oxic littoral to profundal environments. Dolostones, which commonly interbedded and interlaminated with dolomitic/calcareous shales, overlie wackestones or black shales. They were interpreted as littoral deposits in quiet, shallow, and saline lake water during lake contraction (Fig. 3d), in consistent with interpretation from Yang et al. (2007, 2010).

Dolomitic and calcareous shales are interpreted as low-energy and evaporative deposits that mixed detrital grains, dolomite, and calcite, suggesting intermittent clastic deposition and chemical precipitation of carbonate minerals in subaqueous or marginal mud flat. Presence of gypsum suggests relatively high salinity in lake water. In addition, mud

cracks, micro faults, and wrinkly laminae were probably caused by dehydration and fracture of salt-indurated crust in relatively arid conditions. The couplets of organic-rich and dolomitic/calcareous laminae suggest highly variable periods of deposition, and possibly seasonal climate. This is also in accordance with interpretation from Yang et al. (2007, 2010). Organic-rich laminae may have been formed as increased mud influx during wet periods, whereas dolomitic and calcareous laminae may have been formed as reduced mud influx and increased evaporation during dry periods. Dolomitic and calcareous shales commonly overlie wackestone with a gradual contact, and commonly overlain by the transgressive siltstone and sandstone with sharp contact, suggesting they were deposited in littoral environments during late regression (Fig. 3d).

Stacking of the four lithofacies shows systematic changes of lacustrine environments, indicating lake expansion and contraction cycles. These are similar to fluctuating profundal mixed carbonate-siliciclastic high-order cycles described by Yang et al. (2010). The basal part of a high-order cycle contains Lithofacies-I of sandstones and siltstones, which overlies paleosols with a sharp to slightly erosional base. Lithofacies-I is interpreted as transgressive lake plain to littoral deposit, and underlies Lithofacies-II of black shales in sublittoral to profundal environments. This stacking pattern suggests a deepening-upward trend during lake expansion. Upsection, the black shale is overlain by Lithofacies-III of wackestone and dolostone with a sharp contact, which, in turn, is overlain by Lithofacies-IV of dolomitic and calcareous shales. This succession is interpreted as a shallowing-upward environmental trend during lake contraction. However, paleosols are not present on top of Lithofacies-IV in the four high order cycles of this study, although they cap some other high-order cycles in the Lucaogou Formation (Yang et al., 2010). The systematic environmental changes upsection indicate lake shoreline transgression and regression during lake expansion and contraction, which were likely caused by lake level rise and fall, respectively. Finally, Yang et al. (2010) speculated that the lake level fluctuations may have been caused by intra-cyclic climatic changes from humid-subhumid during lake expansion to semi-arid and arid during lake contraction.

5.2. Organofacies and depositional conditions

Multiple bulk geochemical and biomarker proxies have been used to interpret organic matter origins and depositional conditions of the organofacies in the four high-order cycles (Tables 3 and 4). These bulk geochemical and biomarker proxies suggest that the four organofacies may have diverse organic matter origins (Fig. 6c–f and 7a–d), whereas they may have deposited in very similar paleoenvironments of dysoxic and fresh lakewater conditions (Fig. 7e and f).

5.2.1. Organofacies

Geochemical analyses have been conducted to identify organofacies and interpret depositional conditions (Figs. 8–10). The interpretations of depositional condition and sedimentary processes have been compared with those interpreted from field and petrographic evidences.

Organofacies-I may have low primary productivity and terrestrial higher-plant organic matter. A low TOC value (≤1 wt%) suggests low primary productivity, considering good preservation of organic matter and relatively low sedimentation rate of organofacies-I. Good preservation condition is substantiated by microscopic observation of intact woody material (Fig. 5c–e) and biomarker indication of dysoxic lakewater condition (Fig. 7e). A relatively low siliciclastics sedimentation rate is demonstrated by deposition of coarse siltstone and very fine sandstone. In addition, organofacies-I is enriched in ^{13}C, suggesting weak fractionation of ^{12}C from ^{13}C in photosynthesis, as a result of low primary productivity in the lake. This point is also supported by a strong negative correlation between TOC and $\delta^{13}C_{org}$ values (Fig. 6e), although many factors may affect organic carbon isotopic composition of a bulk sediment sample (Hayes, 1993; Tyson, 1995). Stable organic carbon isotope ($\delta^{13}C_{org}$) can be used to indicate not only origin and productivity of organic matter, but also paleoenvironmental condition, on the basis of significant isotopic fractionation generated during photosynthesis that different organisms discriminately using light ^{12}C (Cerling, 1984; Tissot and Welte, 1984; Meyers, 1997). As a result, the organic carbon is more depleted in ^{13}C with a high primary productivity, as plants discriminate against ^{13}C in production of their tissues during photosynthesis. The C_3 higher plants generate (through Calvin pathway) organic matter with a mean $\delta^{13}C_{org}$ value of −27 ‰ in the range between −22 and −34 ‰, whereas lake-derived organic matter that generated by phytoplankton (C_3 algae) has a similar $\delta^{13}C_{org}$ value of −27 ‰ as C_3 plants have in the surrounding watershed, using dissolved CO_2 in isotopic equilibrium with the atmosphere (Craig, 1953; Cerling, 1984; O'Leary, 1988; Meyers, 1997). Organofacies-I consists of Type-III kerogen, as indicated by low H/C ratios and low C/N ratios (Tissot and Welte, 1984; Meyers and Ishiwatari, 1993; 2003). Dominance of long-chain *n*-alkanes and high TAR also suggest organic matter of organofacies-I was mainly derived from terrestrial higher plant, with a few from aquatic macrophytes and algae (Fig. 7a and b; Eglinton and Hamilton, 1967; Rieley et al., 1991; Meyers and Ishiwatari, 1993; Bush and McInerney, 2013). A similar result is suggested by the relative abundance of regular steranes $C_{29} > C_{28} > C_{27}$ on a ternary diagram (Fig. 7c; Huang and Meinschein, 1979; Hakimi and Ahmed, 2016). This is consistent with microscopical

Table 4
Selected geochemical proxies that are not workable to differentiate organofacies.

Geochemical proxies	Proxy information	References
Carbon preference index (CPI)	Maturity and sources of organic matter	Bray and Evans (1961)
Odd even preference (OEP)	Maturity and sources of organic matter	Scalan and Smith (1970)
Pristane/Phytane (Pr/Ph)	Pr was preserved in initial oxidation and Ph was preserved in initial reduction, the ratio is a redox parameter with limitation	Didyk et al. (1978); Peters et al. (2005); Powell, 1987
Tetraterpenoid β-carotane	Reducing conditions involving salinity stratification, evaporative conditions	Hall and Douglas (1983); Brassell et al. (1988); Peters et al. (2005)
Hopanes	Contributions of bacterial membranes, fungi, and cyanobacteria	Ourisson et al. (1979); Rohmer et al. (1992); Ourisson and Albrecht, 1992
Homo-hopane index	Redox conditions, salinity, and biodegradation	Peters and Moldowan (1991); Peters and Moldowan. (1993)
Gammacerane index	Salinity stratified or redox stratified water columns, evaporate or high-salinity environments	Sinninghe Damsté et al., 1995; Sepúlveda et al. (2009); Ritts et al. (1999); Hanson et al. (2000), 2001; Manzi et al. (2007)
Ts/(Ts + Tm) ratio	Maturity, salinity, and source input	Seifert and Moldowan (1978); Moldowan et al. (1986); Rullkötter and Marzi (1988)
Diasteranes index	Thermal maturation, redox condition, and source rock composition (carbonate vs siliciclastic)	Peters et al. (2005); Mello et al. (1988)
C_{29} steranes 20S (20S + 20R)	Thermal maturation, organofacies, weathering, and biodegradation	Seifert and Moldowan (1986); Rullkötter and Marzi (1988); Peters et al. (2005)
C_{29} steranes αββ/(ααα+ αββ)	Thermal maturation, source input, and depositional environment	Seifert and Moldowan (1986); Rullkötter and Marzi (1988)
C_{30} moretanes/ hopane	Thermal maturation, source input, and depositional environment	Seifert and Moldowan, 1980; Rullkötter and Marzi (1988)

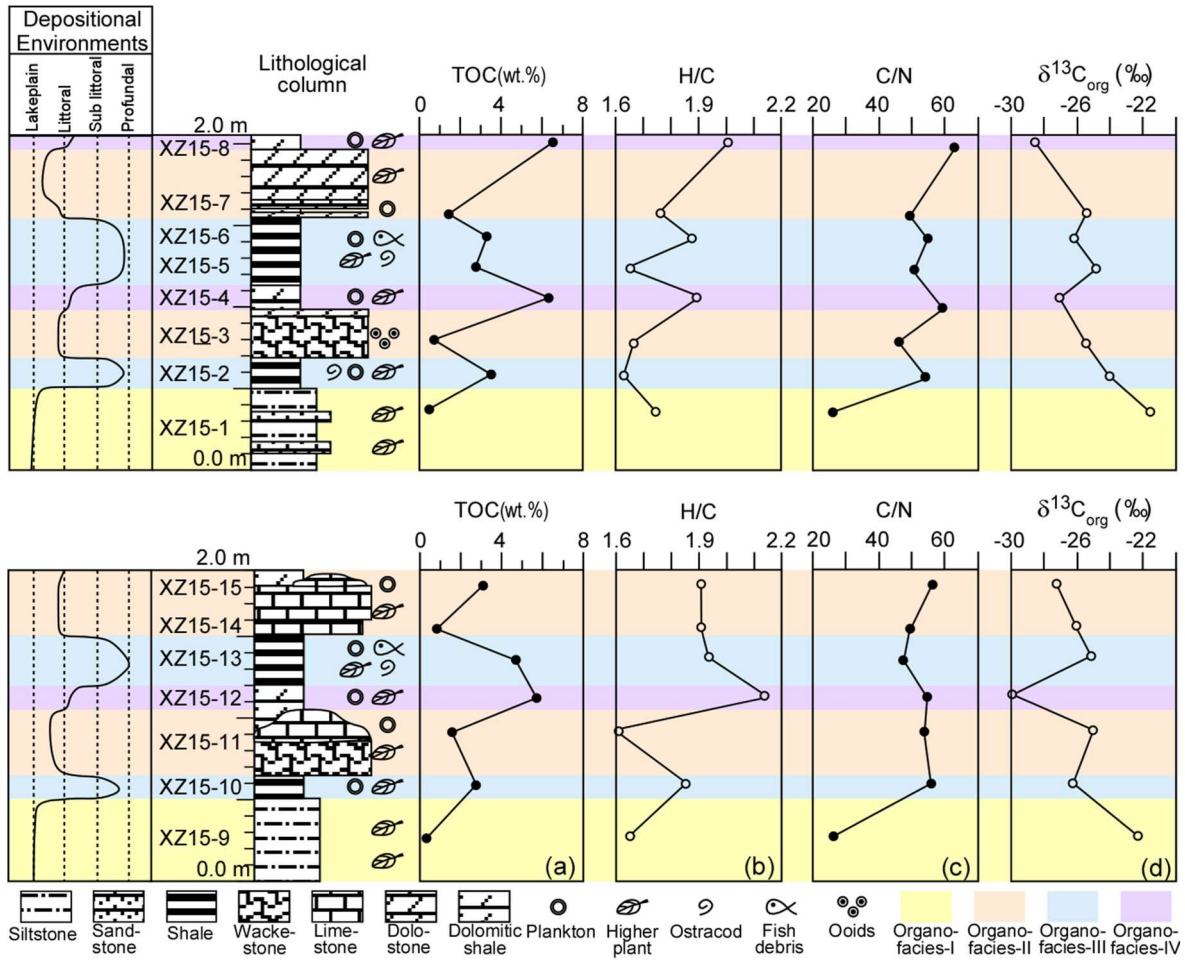

Fig. 8. Four lithofacies are differentiated by (a) content of quartz and feldspar (plagioclase and K-feldspar) v.s. content of calcite and dolomite from XRD results. Four organofacies are differentiated by plots of (b) total organic carbon (TOC) content and calcite equivalent content ($CaCO_3$ %); (c) TOC and hydrogen over carbon ratio (H/C); (d) TOC and ratio of carbon over nitrogen (C/N); (e) TOC content and stable organic carbon isotope ratio ($\delta^{13}C_{org}$); and (f) C/N and $\delta^{13}C_{org}$.

observations of abundant phytoclasts and spores and sparse amorphous organic matter. A low hopane/sterane ratio of organofacies-I implies minor input of bacterial organic matter, because hopanes are typically derived from prokaryotes, while steranes are essentially originated from all eukaryotes (Fig. 7d; Ourisson et al., 1979; Rohmer et al., 1992; Volkman, 2003, 2005).

Oragnofacies-II may have high primary productivity. Organic matter of organofacies-II may have been mainly derived from algae, with some from higher plant and bacteria. A high TOC value (3–5 wt.%) points toward high primary productivity, regarding a similar dysoxic preservation condition and a lower sedimentation rate of black shale in comparison with organofacies-I. Dysoxic lakewater is revealed by well-preserved amorphous organic matter, phytoclasts, spores, and fossils under microscopes (Fig. 5g–i), low Pr/Ph ratio, and high homohopane index (Fig. 7e). Additionally, $\delta^{13}C_{org}$ value of oragnofacies-II is higher than the mean value $\delta^{13}C_{org}$ of −27 ‰ for C_3 plants, suggesting relatively strong fractionation of ^{12}C from ^{13}C in photosynthesis, as a result of very high bioproductivity in the lake. This is evidenced by the negative correlation between TOC and $\delta^{13}C_{org}$ values (Fig. 6e). Oragnofacies-II mainly contains a mixture of organic matter from plankton and higher plant, as revealed by moderate H/C ratios and high C/N ratios (Tissot and Welte, 1984; Meyers and Ishiwatari, 1993; 2003). Moderate TAR and dominance of short-chain *n*-alkanes, with high proportions of long-chain *n*-alkanes, suggest organic matter of oragnofacies-II was mainly derived from algae, with a large amount of others from higher plant (Fig. 7a and b; Meyers and Ishiwatari, 1993; Bush and McInerney, 2013). This is in accordance with proportion of regular steranes $C_{27} > C_{28} > C_{29}$ on a ternary diagram (Fig. 7c; Huang and Meinschein, 1979; Hakimi and Ahmed, 2016). A suchlike result is reinforced by a mixture of abundant amorphous organic matter and phytoclasts observed under stereo- and polarizing microscopes (Fig. 5g–i). A moderate hopane/sterane ratio indicates bacterial organic matter input to oragnofacies-II (Fig. 7d; Ourisson et al., 1979; Rohmer et al., 1992; Volkman, 2003, 2005).

Organofacies-III may have moderate primary productivity. Organic matter of organofacies-III may have been produced by macrophytes and algae, and some others may have been derived from bacteria or strongly affected by microbial modification. A moderate TOC value (1–3 wt.%) suggests moderate primary productivity, taking into account of dysoxic lakewater for organic matter preservation, which is alike in all the four organofacies (Fig. 7e). Moreover, $\delta^{13}C_{org}$ value of oragnofacies-III is close to the mean value $\delta^{13}C_{org}$ of −27 ‰ for C_3 plants, indicating moderate bioproductivity of organofacies-III. Moderate H/C ratios and high C/N ratios imply organic matter of organofacies-III were from both aquatic phytoplankton and terrestrial higher plant (Tissot and Welte, 1984; Meyers and Ishiwatari, 1993; 2003). Moderate TAR and predominance of mid-chain *n*-alkanes with large proportions of short-chain *n*-alkanes suggest organic matter was mainly derived from macrophytes, with a great deal of other from algae (Fig. 7a and b; Meyers and Ishiwatari, 1993; Ficken et al., 2000; Bush and McInerney, 2013). Regular steranes $C_{28} \geq C_{27} > C_{29}$ on a ternary diagram suggest a similar result (Fig. 7c; Huang and Meinschein, 1979; Hakimi and Ahmed, 2016).

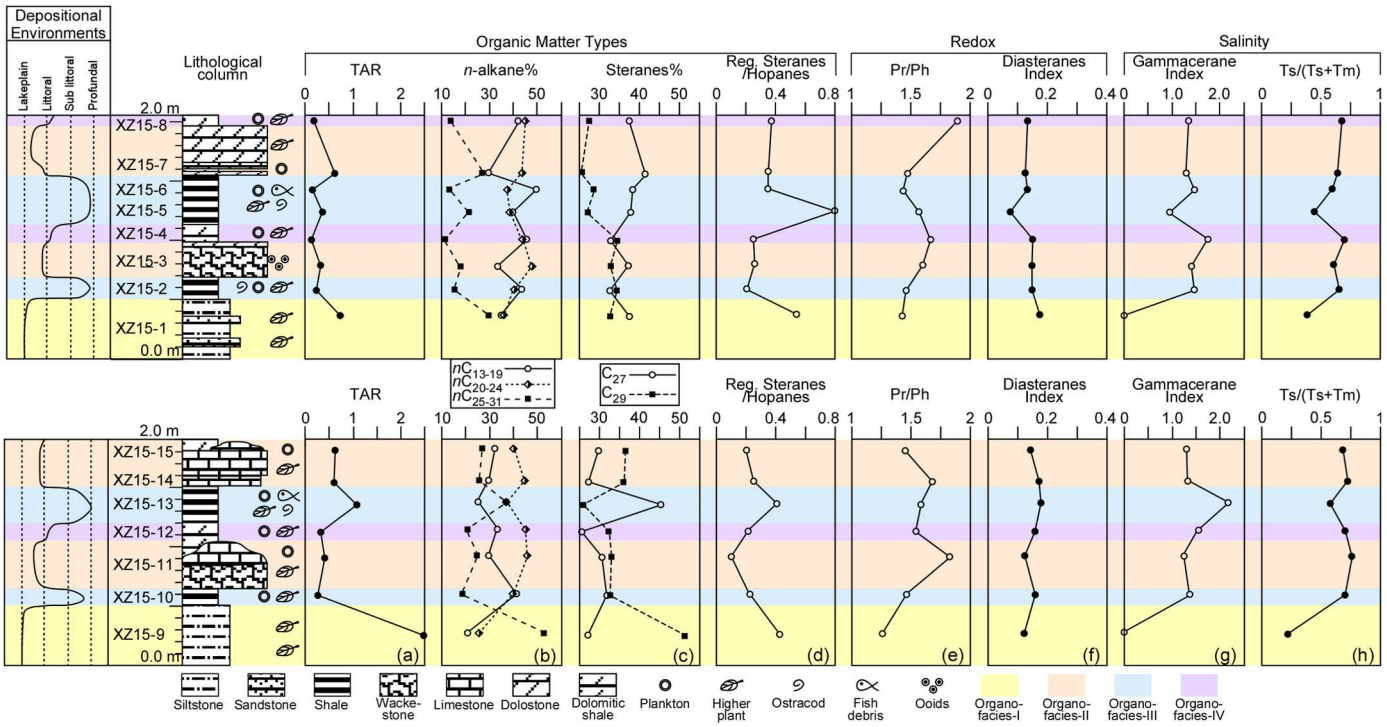

Fig. 9. Four types of organofacies (OF) are differentiated by (a) plots of total organic carbon (TOC) and terrestrial aquatic ratio (TAR); (b) ternary diagram of proportions of short-chain, mid-chain, and long-chain *n*-alkanes; (c) ternary diagram of proportions of regular steranes $C_{27\text{-}29}$, modified after (Hakimi and Ahmed, 2016; Huang and Meinschein, 1979); (d) plots of TAR and ratio of 17-α hopanes over regular steranes $C_{27\text{-}29}$; (e) plots of Homohopane Index and pristane/phytane ratio (Pr/Ph); Homohopane index is calculated as peak areas of C_{35} 17α,21β,(22R + 22S)-pentakishomohopanes over peak areas of C_{33} counterparts; (f) plots of Gammacerane Index and Ts/(Ts + Tm) ratio; Gammacerane Index = 10×gammacerane/(gammacerane + C_{30} 17α(H),21β(H)-hopane); Ts = C_{27} 18α-trisnor-hopane; Tm=C_{27} 17α-trisnor-hopane; (g) plots of TAR and Ts/(Ts + Tm) ratio; (h) plots of C_{29} αββ/(αββ+ααα) ratio and C_{29} 20S/(20S + 20R) ratio; C_{29} 20Sααα = 20S-24-ethyl-5α,14α,17α-cholestane; C_{29} 20Rααβ = 20R-24-ethyl-5α,14β,17β-cholestane; C_{29} 20Sααβ = 20S-24-ethyl-5α,14β,17β-cholestane; C_{29} 20Rααα = 20R-24-ethyl-5α,14α,17α-cholestane; (i) plots of Ts/(Ts + Tm) ratio and ratio of C_{30} 17α,21β-hopane over C_{30} 17β,21α-moretane (C_{30}-hopane βα/αβ).

Moderate to high hopane/sterane ratios of organofacies-III signify nonnegligible input of bacterial material or strong microbial modification on higher-plant and algal organic matter during early deposition (Fig. 7d; Ourisson et al., 1979; Rohmer et al., 1992; Volkman, 2003, 2005). These results are also confirmed by common algae, algal laminae, and phytoclasts, and sparse cyanobacteria observed under polarizing microscope (Fig. 5o and p).

Organofacies-IV may have extremely high primary productivity. A great amount of algae and a few macrophytes may have contributed to organic matter of organofacies-IV. Extremely high primary productivity is suggested by extremely high TOC values (≥5 wt%) of organofacies-IV, under a similarly low sedimentation rate of black shale and dolomitic shale, as well as similarly dysoxic preservation condition of organic matter. Extremely enriched ^{12}C in organofacies-IV indicates strong fractionation of ^{12}C from ^{13}C in photosynthesis, as a consequence of high bioproductivity in the lake. This is congruent with the negative relationship between TOC and $\delta^{13}C_{org}$ values (Fig. 6e). Furthermore, a mixture of plankton and higher-plant organic matter constitutes organofacies-IV, as evidenced by moderate H/C ratios and high C/N ratios (Tissot and Welte, 1984; Meyers and Ishiwatari, 1993; 2003). Low TAR and dominance of short-chain and mid-chain *n*-alkanes in organofacies-IV point out major origins of organic matter from plankton and macrophyte (Fig. 7a and b; Meyers and Ishiwatari, 1993; Ficken et al., 2000; Bush and McInerney, 2013). The same result is evidenced by the proportions of regular steranes $C_{28} > C_{27} \geq C_{29}$ on a ternary diagram (Fig. 7c; Huang and Meinschein, 1979; Hakimi and Ahmed, 2016). This is also substantiated by microscopic observation of abundant amorphous organic matter and well-preserved algae, with common phytoclasts (Fig. 5q–s). A moderate hopane/sterane ratio indicates a small number of bacterial organic matter in organofacies-IV (Fig. 7d; Ourisson et al., 1979; Rohmer et al., 1992; Volkman, 2003, 2005).

However, geolipids constitute only a small fraction of total organic matter, and their origins may not be representative of the dominant material (i.e., mineral composition). Even biomarker compounds, which are relatively resistant to microbial alteration, are subject to diagenetic overprinting that can bias their source information (Meyers, 1997). We emphasize that we do not regard each geochemical index as single, definitive indicator of the organic matter origins and water chemical conditions of the paleoenvironments. Because sediments are not only controlled by deposition, but also altered by biological effect and diagenesis. Consequently, care must be taken using single source-related, environments-related, and maturity-related proxies. A reasonable assessment need to be quantitatively taken with all the independent geochemical indices and petrographic evidences.

5.2.2. *Abundance and organic matter origin*

The C/N ratio is a common proxy for higher-plant organic matter with a ratio ≥20 and plankton with a ratio ≤10 (Meyers, 1997). The C/N ratio has been suggested to have a positive relationship with the TOC value (Ishiwatari and Uzaki, 1987), lignin concentration, and content of $C_{25\text{-}31}$ *n*-alkanes (Prahl et al., 1994), and strong negative relationship with $\delta^{13}C_{org}$ value (Jasper and Gagosian, 1990). However, the C/N ratio has an opposite trend with relative abundance of long-chain *n*-alkanes and TAR value in the four high-order cycles (Fig. 8c and 9a–b). In addition, the C/N ratio is irrelevant with the TOC value (Fig. 6d) and weakly correlated with the $\delta^{13}C_{org}$ value (Fig. 6f). The determination of organic matter origins using the C/N ratio thus appears unreliable, especially for a mixture of plankton and higher-plant organic matter. Consequently, it is inappropriate to distinguish plankton and higher-plant organic matter solely on the C/N ratio, without considering

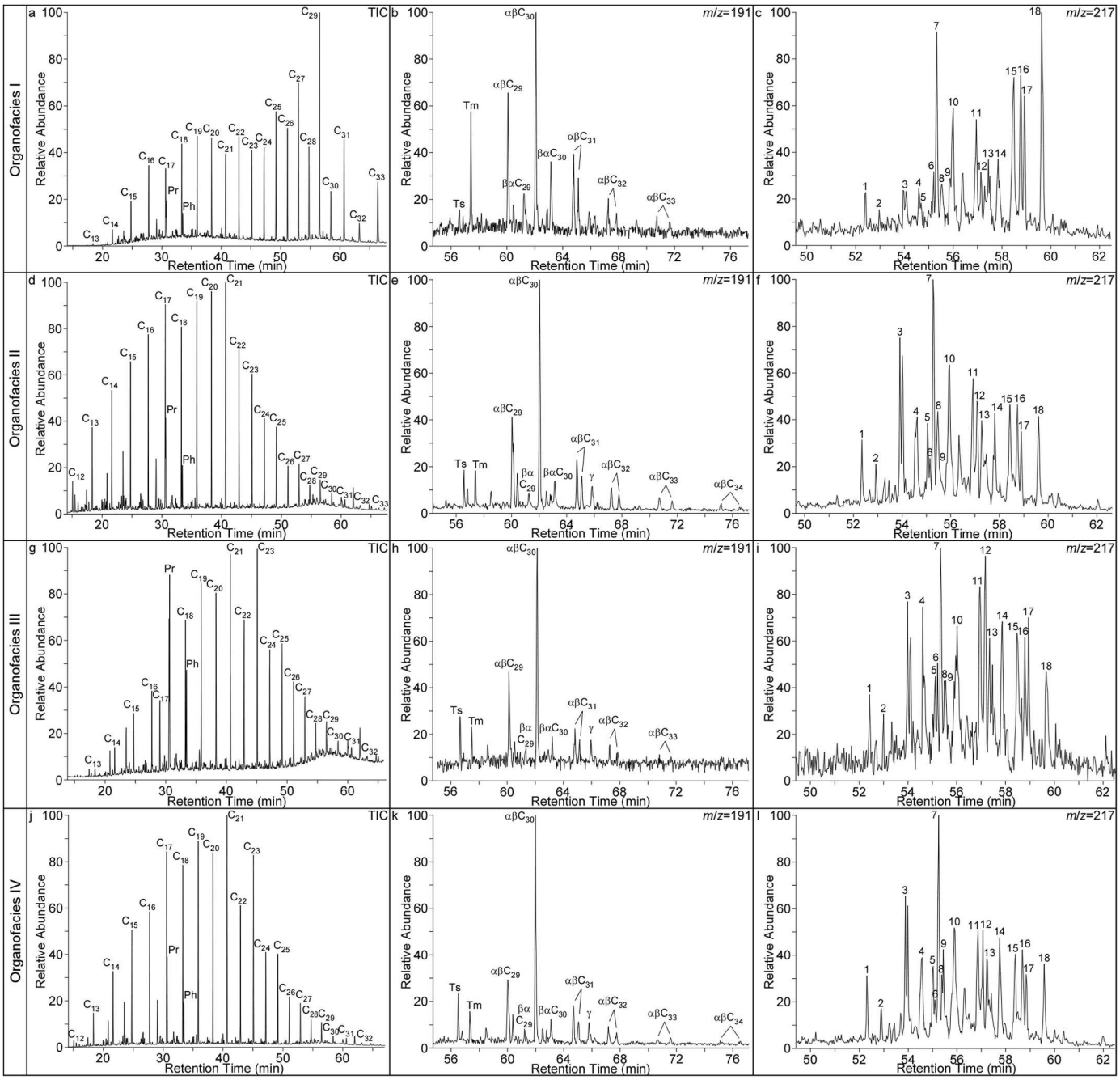

Fig. 10. Representative mass chromatograms of *n*-alkanes (TIC), hopanes (*m/z* = 191), and steranes (*m/z* = 217) from four organofacies. Ts = 18α-22,29,30-Trisnorneohopane; Tm = 17α-22,29,30-Trisnorhopane; αβ29 = 17α,21β-30-Norhopane; βα29 = 17β,21α-30-Normoretane; αβ30 = 17α,21β-Hopane; βα30 = 17β,21α-Moretane; αβ31 = 22S&R-17α,21β-Homohopane; Ga = Gammacerane; αβ32 = 22S&R-17α,21β-Bishomohopane; αβ33 = 22S&R-17α,21β-Trishomohopane; αβ34 = 22S&R-17α,21β-Tetrashomohopane; 1 = 20S-13β,17α-Diacholestane; 2 = 20R-13β,17α-Diacholestane; 3 = 20S-24-Methyl-13β,17α-cholestanes; 4 = 20R-24-Methyl-13β,17α-cholestanes; 5 = 20S-5α,14α,17α-cholestane; 6 = 20R-5α,14β,17β-cholestane; 7 = 20S-24-Ethyl-13β,17α-cholestanes; 8 = 20S-5α,14β,17β-cholestane; 9 = 20R-5α,14α,17α-cholestane; 10 = 20R-24-Ethyl-13β,17α-cholestanes; 11 = 20S-24-Methyl-5α,14α,17α-cholestanes; 12 = 20R-24-Methyl-5α,14β,17β-cholestanes; 13 = 20S-24-Methyl-5α,14β,17β-cholestanes; 14 = 20R-24-Methyl-5α,14α,17α-cholestanes; 15 = 20S-24-Ethyl-5α,14α,17α-cholestanes; 16 = 20R-24-Ethyl-5α,14β,17β-cholestanes; 17 = 20S-24-Ethyl-5α,14β,17β-cholestanes; 18 = 20R-24-Ethyl-5α,14α,17α-cholestanes.

proportions of aquatic and terrestrial organic matter, soil organic matter with low C/N ratios (e.g., Zhao et al., 2015), and terrestrial organic matter with low C/N ratios.

The relative abundance of the C_{27} steranes has a similar trend, although not exactly the same, with that of the short-chain *n*-alkanes, while content of the C_{29} steranes have a similar trend with that of the long-chain *n*-alkanes in the lower two high-order cycles (Fig. 9b and c). Contradictorily, proportion of the C_{27} steranes has an opposite trend with that of the short-chain *n*-alkanes, while proportion of the C_{29}-steranes has a contrary trend with that of the long-chain *n*-alkanes in the upper two high-order cycles (Fig. 9b and c). This contradiction may be explained by an alternative interpretation of the dominance of the long-chain *n*-alkanes and the C_{29} steranes.

Distribution and abundance of *n*-alkanes may indicate organic matter type and maturity (Peters et al., 2005). However, absolute amounts of terrestrial organic matter might be disproportionately overestimated using *n*-alkanes, as land plants typically contain higher proportions of *n*-alkanes than those of aquatic organisms (Cranwell et al., 1987;

Goossens et al., 1989; Meyers and Ishiwatari, 1993). In addition, lacustrine algae (e.g. Botryococus braunii) may contribute to the C_{27}–C_{33} *n*-alkanes. (Moldowan et al., 1985; Derenne et al., 1988; Liu et al., 2018). Furthermore, some *n*-alkanes are also sensitive to thermal maturation and biodegradation (Tissot and Welte, 1984). Nonetheless, relative abundance of short-chain *n*-alkanes have a similar trend with the H/C ratio and an opposite trend with the relative abundance of long-chain *n*-alkanes and TAR in the four high-order cycles (Fig. 8b and 9a–b), suggesting *n*-alkanes is valuable for determining changes in contribution of organic matter from terrestrial or aquatic systems.

Proportions of $C_{27\text{-}29}$ regular steranes have been utilized to differentiate plankton and higher-plant organic matter and their depositional environments (Huang and Meinschein, 1979; Moldowan et al., 1985). C_{27} steranes are predominately derived from microalgae (e.g. Eustigmatophyceae and Haptophyceae; Volkman et al., 1998; Volkman, 2003). C_{28} steranes typically constitute the sterols of specific microalgae (e.g., diatom, Haptophyceae, Cryptophyceae, Chrysophyceae, and Chlorophyceae; Goad et al., 1983; Volkman, 1986), fungi (Méjanelle et al., 2000), and leaf waxes in higher plants (Rieley et al., 1991; Volkman, 2003). C_{29} steranes are principally associated with the sterol composition of vascular plants (Volkman, 1986; Rieley et al., 1991). However, C_{29} steranes have been also reported in specific freshwater microalgae (e.g., Chrysophyceae, Eustigmatophyceae, Chlorophyceae, and Prasinophyceae; Volkman et al., 1998; Kodner et al., 2008) and cyanobacteria (Volkman, 1986, 2003, 2005). Accordingly, the contribution from terrestrial higher plant to organic matter might have been overrated.

5.2.3. Depositional conditions

Redox condition of water column is an integrated effect of oxygen cycling in biosphere, atmosphere, and geosphere in a lake system. Oxygen is depleted by biological and inorganic oxidation and is supplied with the input of oxygenated waters from fluvial systems, via exchange with atmosphere and as byproduct of photosynthesis. Lakewater redox condition of the four organofacies is overall dysoxic, based on the redox-related biomarker parameters of pristane over phytane ratio (Pr/Ph), homohopane index, and diasterane index. A similar redox condition of all the samples in the high-order cycles suggest lithofacies may not be reliable to interpret redox condition and geochemical proxies related to redox condition may not be appropriate to classify organofacies in this study.

The Pr/Ph ratio has been generally considered as a redox parameter for anoxic (Pr/Ph $\leq$ 1) and oxic conditions (Pr/Ph $\geq$ 3; Didyk et al., 1978). The Pr/Ph ratio of all samples in the four organofacies is in a narrow range of 1.3–1.9 (Fig. 7e), suggesting the samples were likely deposited in dysoxic lakewater. However, Pr/Ph ratios between 1 and 3 are not recommended for determining redox condition of depositional environments (Peters et al., 2005). The Pr/Ph ratios are known to be affected by maturation (Tissot and Welte, 1984) and by differences in precursors for acyclic isoprenoids (Volkman and Maxwell, 1986; ten Haven et al., 1987). Thermal diagenesis favors preservation of pristane to phytane, result in an increasing Pr/Ph value with maturity (Didyk et al., 1978). Volkman (1988) also suggests that archaebacteria and haloalkaliphilic bacteria can be important sources of phytane.

Low homohopane index (C_{35} homo-hopanes over $C_{33\text{-}34}$ homologues) of 0.1–0.5 in all the samples from the four organofacies suggest a generally dysoxic water body in the lake (Fig. 7e). A low abundance of homohopane has been empirically used to imply oxic depositional environment (Peters and Moldowan, 1993). However, the ratio of C_{35} to $C_{33\text{-}34}$ homo-hopanes may be influenced by thermal maturation, biodegradation, and sulfur availability in depositional environments (Peters and Moldowan, 1991). Nevertheless, a good correlation between the homohopane index and Pr/Ph ratio of the four organofacies indicates the lakewater was dysoxic (Fig. 7e), as also supported from microscopic evidence of good preservation of organic matter and aragonitic skeletal fragments.

Diasterane index increases with increasing maturity (equilibrium of ~0.36), as diasteranes are more stable than regular steranes (Peters et al., 1990). It is typically used to distinguish organic matter from carbonate versus clastic depositional environments, as acidic (low pH) and oxic (high Eh) conditions facilitate formation of diasterenes (Moldowan et al., 1986; Mello et al., 1988). In consideration of a similar thermal maturity of the samples in the meter-scaled high-order cycles, low diasterane index values of 0.09–0.18 in all the samples may suggest dysoxic environments (Table 2). Alternatively, low values of diasteranes index may be interpreted as clay-poor or carbonate rock that was deposited in high pH and low Eh conditions, in which calcite is promoted to precipitate and organic matter is preserved. But this is contradicted to the lowest diasterane index value of black shales in the upper high-order cycles and siltstones in the lower high-order cycles (XZ15-5, XZ15-9; Fig. 9f).

Multiple salinity-related biomarker parameters of samples in the four organofacies reveal that they were probably deposited in fresh lakewater environments. Gammacerane index is widely used as a proxy of salinity. It may be associated with planktonic and bacteriovorous ciliates (Grice et al., 1998), which occur at the interface between oxic and anoxic zones in stratified water columns (Sinninghe Damsté et al., 1995; Sepúlveda et al., 2009). A high abundance of gammacerane usually typifies evaporitic or high-salinity environments, as a result of stratified water columns (Fu et al., 1986, 1990; Ritts et al., 1999; Hanson et al., 2000, 2001; Manzi et al., 2007). Gammacerane is present in all the samples, with gammacerane index in the range of 0–2.2, except for two samples from organofacies-I, in which gammacerane is too low to be detected (Table 2). Absence or a low abundance of gammacerane suggests all the samples in the high-order cycles were deposited in fresh lakewater.

The tetraterpenoid hydrocarbon β-carotane is considered to be formed in highly reducing conditions involving salinity stratification, shallow and evaporative lake, and highly restricted marine environments, due to blooming of specific classes of algae and bacteria during widespread desiccation in an arid climatic interval (Hall and Douglas, 1983; Brassell et al., 1988; Peters et al., 2005). Carroll et al. (1992) found abundant β-carotane in a desiccated interval in the marginal facies but minor quantities in the basinal facies at base of the Tianchi section and Urumqi section of the Lucaogou Formation. Trace β-carotane is present in two black shales and two dolostones, but absent in the other samples in the high-order cycles (Table 2), indicating the four organofacies were probably deposited in fresh lakewater. This is consistent with records of gammacerane of the four organofacies.

A Ts/(Ts + Tm) ratio is generally considered as one of the most reliable indicators for maturity assessment, as 8α-22,29,30-trisnorneohopane-C_{27} (Ts) is more stable than 17α-22,29,30-trisnorhopane-C_{27} (Tm) during catagenesis (Seifert and Moldowan, 1978; Peters et al., 2005). In addition, the Ts/(Ts + Tm) ratio may be used as a salinity-sensitive proxy, when samples have similar thermal maturity, because Ts/(Ts + Tm) ratios increase in hyper-saline depositional environments (Moldowan et al., 1986; Rullkötter and Marzi, 1988; Peters et al., 2005). In this study, organic matter maturity should be similar in the meter-scale high-order cycles. It is noteworthy that a good positive correlation exists between the gammacerane index and Ts/(Ts + Tm) ratio of all the samples (Fig. 7f). Samples from organofacies-I have low Ts/(Ts + Tm) ratios of 0.22–0.33, while the other samples have moderate Ts/(Ts + Tm) ratios of 0.38–0.57 (Table 2). Thus, low Ts/(Ts + Tm) ratios may suggest fresh lakewater environments. Alternatively, the Ts/(Ts + Tm) ratio may be a source-related parameter, because the ratio is partially controlled by source input (Moldowan et al., 1986). The Ts/(Ts + Tm) ratio has a similar trend with the relative abundance of mid-chain *n*-alkanes (Fig. 5b–h) and an opposite pattern with the TAR, long-chain *n*-alkanes, C_{29}-steranes, and steranes/hopanes ratio in the high-order cycles (Fig. 5a–d). It is further confirmed by a good negative correlation between the Ts/(Ts + Tm) ratio and TAR (Fig. 7g). Consequently, an alternative interpretation of low Ts/(Ts + Tm) ratio is

organic matter input of specific macrophytes or sphagnum, with possible microbial modification during deposition.

5.3. Organic matter maturity

A verities of maturity-sensitive indicators suggest the four organofacies are early mature, including carbon preference index (CPI), odd even preference (OEP), ratio of ββ/(ββ+αα) stereotypes in C_{29} steranes, ratio of 20S/(20S + 20R) stereochemistry in C_{29} steranes, and ratio of C_{30} 17β,21α-moretane over C_{30} 17α,21β-hopane (C_{30}-hopane βα/αβ). This view is in agreement with the assumption that all the samples in the meter-scale high-order cycles should be at similar maturity.

As a maturity indicating proxy, CPI of *n*-alkanes was introduced by Bray and Evans (1961) and improved as OEP by Scalan and Smith (1970). The CPI or OEP values significantly above or below 1.0 indicate immaturity, whereas values of 1.0 suggest mature organic matter (Peters et al., 2005). Relatively high CPI values of 1.2–2.1 and high OEP values of 1.2–1.6 in the four organofacies suggest the samples are immature to early mature "oil window" (Table 2).

Isomerization at C-20 in C_{29} 5α,14α,17α-steranes causes an increase of 20S/(20S + 20R) ratio with increasing thermal maturity (equilibrium of 0.52–0.55), while isomerization at C-14 and C-17 in the C_{29} 20S and 20R regular steranes promotes an increase of ββ/(ββ+αα) ratio with increasing thermal maturity (equilibrium of 0.67–0.71; Seifert and Moldowan, 1986). In all the samples of the four high-order cycles, C_{29} 20S/(20S + 20R) ratio range is 0.36–0.60, with a mean value of 0.50, while C_{29} ββ/(ββ+αα) ratio ranges in 0.30–0.51, with a mean value of 0.42, suggesting the four organofacies are early mature to mature (Table 2). However, plots of C_{29} 20S/(20S + 20R) and ββ/(ββ+αα) ratios of the samples are deviated from the maturity trend line with irrelevance (Fig. 7h). As a result, overall early mature organofacies are more reasonable, since the maturity is highly overrated based on the 20S/(20S + 20R) and ββ/(ββ+αα) ratios. The disagreement could be induced by different levels of clay catalysis (e.g., Huang et al., 1990) and different organofacies (e.g., Moldowan et al., 1986).

Hopanes in the four organofacies have similar distributions of compounds. These hopanes mainly consist of C_{27} to C_{35} 17α,21β-hopanes, with C_{30}-hopane as the major compound, and low relative abundance of C_{29} to C_{31} 17β,21α-moretanes. The C_{30}-hopane βα/(βα+αβ) ratio is in the range of 0.02–0.28, with a mean value 0.11 in all the samples, suggesting the four organofacies are early mature to mature. The 17α,21β-hopane is thermally more stable than 17β,21α-moretane, as a result, the C_{30}-hopane βα/(βα+αβ) ratio decreases with thermal maturity (equilibrium of 0.13; Seifert and Moldowan, 1986). However, the maturity on account of the hopane βα/(βα+αβ) ratio may be overestimated. Plots of the C_{30}-hopane βα/(βα+αβ) and Ts/(Ts + Tm) ratios of the samples show a strong correlation (Fig. 7i), suggesting they were probably influenced by source inputs or depositional environments (e.g., Rullkötter and Marzi, 1988).

5.4. Relationship between litho- and organo-facies

A genetically associated one-one relationship between litho- and organo-facies is suggested by correlation between litho- and organo-facies (Figs. 8 and 9). Similarities and differences of the four lithofacies and their corresponding four organo-facies are summarized in Table 5. Four organofacies have distinctive chemical composition, organic matter abundance and type, but similar redox condition, lake water salinity, and thermal maturity.

Organofacies-I corresponds to the interbedded and interlaminated coarse siltstone and very fine sandstone (Lithofacies-I). Sediments of silt- and sand-size may have been transported relative short distance from clastic source and deposited in relatively high-energy littoral environments as the lake expended. Organic matter of organofacies-I was mainly originated from higher terrestrial plants, with a few from plankton and macrophytes, and they were probably deposited in lake-plain to littoral environments during the earliest lake extension. The lithofacies and organofacies may have been formed during early shoreline transgression, when the rates of base-level rise just outpaced the rates of sediments and water supply, in a small shallow lake. Higher terrestrial plants were likely developed surrounding the lake, while aquatic plankton was limited during early lake expansion, because of

Table 5
Diagnostic characteristics of lithofacies & organofacies in the four high-order cycles in the Lucaogou Formation.

Lithofacies				Organofacies					
Lithology associations	Sedimentary Structures	Organic matter (OM)&fossils	Depositinal environment	Organo-facies	Geochemical composition	Organic matter	Redox condition	Salinity	Maturity
Interbedded& interlaminated coarse siltstone&very fine sandstone	Weakly laminated, massive, &erosional base	Abundant phytoclasts, spores, sparse amorphous OM	High-energy lake-plain littoral	**Organo-facies-I**	TOC: 0.2–0.3 wt%, H/C: ~1.7, C/N: 25.9–26.3, $\delta^{13}C_{org}$: −22.5 to −21.8 ‰	Low productivity, mainly higher plant, a few plankton & macrophytes	Dysoxic	Fresh lakewater	Early mature
Black shale	Well-parallel sub-mm- to mm-laminated, climbing rippled, & erosional	Abundant phytoclasts amorphous OM, &ostracods	Low-energy profundal	**Oragno-facies-II**	TOC: 2.8–4.8 wt%, H/C: 1.6–1.9, C/N: 40.0–47.8, $\delta^{13}C_{org}$: −26.2 to −24.1‰	High productivity, mainly plankton & higher plants	Dysoxic	Fresh lakewater	Early mature
Wackestone & dolostone	Wrinkly laminated, & parallel laminated	Common algae & phytoclasts, sparse ooids, ostracods, skeletal fragments, & cyanobacteria	Low- to high-energy littoral–sub littoral	**Organo-facies-III**	TOC: 0.7–3.0 wt%, H/C: 1.6–1.9, C/N: 39.5–48.7, $\delta^{13}C_{org}$: −27.2 to −25.1‰	Low productivity, mainly macrophytes, plankton, & bacteria	Dysoxic	Fresh lakewater	Early mature
Dolomitic and calcareous shales	Well-parallel sub-mm- to mm-interlaminated & algal laminated	Abundant amorphous OM, common phytoclasts, spores, sparse ostracods, &gastropods	Low-energy littoral	**Organo-facies-IV**	TOC: 5.9–6.5 wt%, H/C: 1.9–2.1, C/N: 36.4–49.9, $\delta^{13}C_{org}$: −29.6 to −27.3‰	High productivity, mainly plankton, a few macrophytes	Dysoxic	Fresh lakewater	Early mature

restricted lake area and low primary productivity.

Oragnofacies-II is linked with the black shale (Lithofacies-II). Black shales may have been deposited as fine sediments transported relatively remote distance into low-energy profundal environments as the lake expended. Organic matter of oragnofacies-II was derived from plankton and terrestrial higher plants and deposited in profundal environments during the maximum transgression. Oragnofacies-II and black shale may have been developed during the late and maximum shoreline transgression, when rate of base-level rise outstripped rates of sediment and water supply, in a large and deep lake. Algae blooms were likely promoted due to increasing lake area during the lake expansion. Distribution of terrestrial higher plants surrounding the lake was more limited, in comparison with the lake of organofacies-I.

Organofacies-III coincides with the wackestone and dolostone (Lithofacies-III). These carbonates were probably deposited on the condition that sufficient supply of dissolved calcium, magnesium, and CO_2–HCO_3^--CO_3^{2-} in the lake systems, while clastic sediments were limited in restriction of influx. Limited influx of siliciclastic sediments may promote carbonate construction. Organofacies-III has organic matter that were principally derived from macrophytes and algae, and some others from bacteria, and deposited in littoral–sublittoral environments during regression. It may have been generated during the forced regression, when rates of sediment and water supply outpaced rate of base-level fall, in a relatively small shallow lake. Limited influx may not be able to transport a large number of terrestrial plant remains into the lake. Aquatic macrophytes and algae may be accumulated in the lake, but their development may have been constrained by supply and circulation of necessary element (e.g., N, P, Na, and Fe) from the limited influx.

Organofacies-IV is associated with the dolomitic and calcareous shales (Lithofacies-IV). Abundant algae, with a few from macrophytes, contributed to organic matter of organofacies-IV, which was deposited in low-energy lakewater of littoral environments during the latest regression. It may have been produced during the normal regression, when rates of base-level rise were in balance with rates of sediment and water supply, in a small shallow lake. Constant inflow increased as the base level increased during the lake expansion, providing increasing detrital grain supply and causing decreasing carbonate mineral supply. Sufficient nutrient and oxygen supplied by constant influx may have provided appropriate conditions for growth of algae and macrophytes, giving rise to high primary productivity.

Shifts of litho- and organo-facies are synchronous with lake expansion and contraction (Figs. 8 and 9). Litho- and organo-facies in the four high-order cycles may have been oscillated with fluctuation of lake level and shoreline trajectories, in terms of hydrology and sedimentation. Similarly, a high-frequency euxinia (1–10 m scale), likely caused by high bioproductivity in the photic zone of an ancient sea, was reported periodically impinged on the lower slope and in the shallow basin of the Southern Permian basins of northern Pangea (Słowakiewicz et al., 2015, 2016). Curiale et al. (1992), Horsfield et al. (1994), Tyson (1995), Carroll and Bohacs (1999), and Slatt and Rodriguez (2012) also reported a similar result that the changes of organofacies indicate fluctuation of base level and both small and large cycles are related to transgressive-regressive events. Organofacies, characterized by its organic constituents in sediments, is controlled by the nature of primary biomass, extent of bacterial degradation, and reworking during deposition, chemical condition of water body in the depositional environment (Jones and Demaison, 1982; Powell, 1987; Tyson, 1995; Meyers, 2003). However, organofacies in the four high-order cycles are classified, in accordance with specific bulk geochemical parameters related to geochemical composition of organic matter and specific biomarker proxies related to types of organic matter, rather than those related to depositional conditions (e.g., redox condition and lakewater salinity) and thermal maturity. This suggests that geochemical composition and organic matter abundance and type may have been controlled by transgressive-regressive events in high-order cycles, while depositional conditions have been remained unchanged in high-order cycles.

6. Conclusions

A centimeter-scale investigation of mixed carbonate and siliciclastic lacustrine deposits in the Lucaogou high-order cycles shows that litho- and organo-facies are correlated and genetically associated with lake extension and contraction. Four lithofacies including interbedded and interlaminated coarse siltstone and very fine sandstone, black shale, wackestone and dolostone, and calcareous and dolomitic shales have been identified. Four distinctive organofacies have been identified, based on geochemical composition of organic matter and biomarker proxies related to organic matter abundance and type, rather than depositional conditions and thermal maturity.

Organofacies-I is associated with the interbedded and interlaminated coarse siltstone and very fine sandstone. Organic matter of organofacies-I was mainly originated from higher terrestrial plants, with a few from plankton and macrophytes, in lake-plain to littoral environments during the earliest lake extension. Oragnofacies-II is linked with black shale. Organic matter of oragnofacies-II was derived from plankton and terrestrial higher plants and deposited in profundal environments during the maximum transgression. Organofacies-III corresponds to wackestone and dolostone. Organofacies-III has organic matter that were principally derived from macrophytes and algae, and some others from bacteria, and deposited in littoral–sublittoral environments during regression. Organofacies-IV coincides with dolomitic and calcareous shales. Abundant algae, with a few from macrophytes, contributed to organic matter of organofacies-IV, which was deposited in low-energy lakewater in littoral environments during the latest regression.

The four organofacies are associated with four lacustrine lithofacies associations in the 4 m-scale high-order cycles, suggesting litho- and organo-facies are genetically linked and may have been controlled by lake contractions and extensions. The lithofacies-derived and environment-defined high-order cycles can be delineated and substantiated by geochemical proxies-defined organofacies, in terms of organic matter abundance and type. The four organofacies may have been formed in similar conditions of fresh and dysoxic lakewater, indicating that geochemical proxies related to depositional condition may not be used to characterize organofacies in the high-order cycles. This integrated study demonstrates that a holistic approach combining lithofacies and organofacies analyses is useful in reconstruction of depositional processes on meter-scaled cyclic deposits in a lacustrine system.

Declaration of competing interest

The authors declare that they have no known competing financial interests or personal relationships that could have appeared to influence the work reported in this paper.

Data availability

Data will be made available on request.

Acknowledgments

We appreciate Dr. Guoying Sheng, Dr. Hong Lu, Dr. Zewen Liao, Dr. Jing Liao, Dr. Qingtao Wang, and Dr. Taoli Wang of Guangzhou Institute of Geochemistry, Chinese Academy of Sciences for GC-MS facilities and for advices. Thanks to Dr. David Wronkiewicz, Dr. Jonathan Obrist Farner, and Dr. Stephen Gao in Missouri S&T for advices. Thanks to Yiran Lv, Xiaowei Peng, and Ziyue Ju in Missouri S&T for field help. This research was partially supported by four research grants from Geological Society of America, American Association of Petroleum Geologists [M. Ray Thomasson; SEAPEX], and State Key Laboratory of Organic Geochemistry, Chinese Academy of Sciences [grant no. SKLOG-201603]

to Dr. Xin Zhan, NSF EAR grant [1714749] and NSF China grant [41428201] to Dr. Wan Yang, and NSF China grant [41973067] to Dr. Zhao-Wen Zhan. The authors would like to give special thanks to the editors and anonymous reviewers for constructive comments and suggestions which improved the manuscript.

References

American Geological Institute, 1973. Glossary of Geology. American Geological Institute, Washington, D.C, pp. 1–805.
Bohacs, K.M., Carroll, A.R., Neal, J.E., Mankiewicz, P.J., 2000. Lake basin type, source potential, and hydrocarbon character: an integrated sequence-stratigraphic-geochemical framework. In: Gierlowski-Kordesch, E.H., Kelts, K.R. (Eds.), Lake Basins through Space and Time, AAPG Studies in Geology, vol.46, pp. 3–34.
Bourbonniere, R.A., Meyers, P.A., 1996. Sedimentary geolipid records of historical changes in the watersheds and productivities of Lakes Ontario and Erie. Limnol. Oceanogr. 41, 352–359.
Bradley, W.H., 1925. A contribution to the origin of the Green River Formation and its oil shale. AAPG (Am. Assoc. Pet. Geol.) Bull. 9, 247–262.
Brassell, S.C., Eglinton, G., Sheng, G., Fu, J.M., 1988. Biological Markers in Lacustrine Chinese Oil Shales, vol.40. Geological Society, London, Special Publications, pp. 299–308.
Bray, E.E., Evans, E.D., 1961. Distribution of n-paraffins as a clue to recognition of source beds. Geochem. Cosmochim. Acta 22, 2–15.
Brown Jr., L.F., Fisher, W.L., 1977. Seismic-stratigraphic interpretation of depositional systems: examples from Brazilian rift and pull-apart basins. In: Payton, C.E. (Ed.), Seismic Stratigraphy-Applications to Exploration. AAPG Memoirs 26, Tulsa, pp. 213–248.
Bush, R., McInerney, F.A., 2013. Leaf wax n-alkane distributions in and across modern plants: implications for paleoecology and chemotaxonomy. Geochem. Cosmochim. Acta 117, 161–179.
Carroll, A.R., Bohacs, K.M., 1999. Stratigraphic classification of ancient takes: balancing tectonic and climatic controls. Geology 27, 99–102.
Carroll, A.R., Bohacs, K.M., 2001. Lake-type controls on petroleum source rock potential in nonmarine basins. AAPG (Am. Assoc. Pet. Geol.) Bull. 85, 1033–1053.
Carroll, A.R., Brassell, S.C., Graham, S.A., 1992. Upper permian lacustrine oil shales, southern Junggar Basin, northwest China. AAPG (Am. Assoc. Pet. Geol.) Bull. 76, 1874–1902.
Carroll, A.R., Graham, S.A., Hendrix, M.S., 1995. Late Paleozoic tectonic amalgamation of northwestern China: sedimentary record of the northern Tarim, northwestern Turpan, and southern Junggar basins. GSA Bulletin 107, 571–594.
Carroll, A.R., 1998. Upper Permian lacustrine organic facies evolution, southern Junggar Basin, NW China. Org. Geochem. 28, 649–667.
Cerling, T.E., 1984. The stable isotopic composition of modern soil carbonate and its relationship to climate. Earth Planet Sci. Lett. 71, 229–240.
Chen, Z., Wu, N., Zhang, D., Hu, J., Huang, H., Shen, G., Wu, G., Tang, H., Hu, Y., 1985. Geologic Map of Xinjiang Uygur Autonomous Region, Scale 1: 2,000,000. Geologic Publishing House, Beijing, 1 sheet.
Chumakov, N.M., Zharkov, M.A., 2003. Climate during the permian–triassic biosphere reorganizations. Article 2. Climate of the late permian and early triassic: general inferences. Stratigr. Geol. Correl. 11, 361–375.
Cohen, K.M., Finney, S.C., Gibbard, P.L., Fan, J.X., 2013. The ICS international chronostratigraphic chart. Episodes 36, 199–204.
Craig, H., 1953. The geochemistry of the stable carbon isotopes. Geochem. Cosmochim. Acta 3, 53–92.
Craig, H., 1957. Isotopic standards for carbon and oxygen and correction factors for mass-spectrometric analysis of carbon dioxide. Geochem. Cosmochim. Acta 12, 133–149.
Cranwell, P.A., Eglinton, G., Robinson, N., 1987. Lipids of aquatic organisms as potential contributors to lacustrine sediments-II. Org. Geochem. 11, 513–527.
Curiale, J., Lin, R., 1991. Tertiary deltaic and lacustrine organic facies: comparison of biomarker and kerogen distributions. Org. Geochem. 17, 785–803.
Curiale, J.A., Cole, R.D., Witmer, R.J., 1992. Application of organic geochemistry to sequence stratigraphic analysis: Four Corners Platform Area, New Mexico, U.S.A. Advances in. Org. Geochem. 19, 53–75.
Derenne, S., Largeau, C., Casadevall, E., Connan, J., 1988. Comparison of torbanites of various origins and evolutionary stages. Bacterial contribution to their formation. Cause of lack of botryococcane in bitumens. Org. Geochem. 12, 43–59.
Didyk, B.M., Simoneit, B.R.T., Brassell, S.C., Eglinton, G., 1978. Organic geochemical indicators of palaeoenvironmental conditions of sedimentation. Nature 272, 216–222.
Durand, B., Nicaise, G., 1980. Procedures for kerogen isolation. In: Durand, B. (Ed.), Kerogen-Insoluble Organic Matter from Sedimentary Rocks. Editions Technip, Paris, pp. 35–53.
Eglinton, G., Hamilton, R.J., 1967. Leaf epicuticular waxes. Science 156, 1322–1335.
Ficken, K.J., Li, B., Swain, D.L., Eglinton, G., 2000. An *n*-alkane proxy for the sedimentary input of submerged/floating freshwater aquatic macrophytes. Org. Geochem. 31, 745–749.
Fu, J., Sheng, G., Peng, P., Brassell, S.C., Eglinton, G., Jiang, J., 1986. Peculiarities of salt lake sediments as potential source rocks in China. Org. Geochem. 10, 119–126.
Fu, J., Sheng, G., Xu, J., Eglinton, G., Gowar, A.P., Jia, R., Fan, S., Peng, P., 1990. Application of biological markers in the assessment of paleoenvironments of Chinese non-marine sediments. Org. Geochem. 16, 769–779.
Gierlowski-Kordesch, E.H., Kelts, K.R., 1994. Introduction. In: Gierlowski-Kordesch, E., Kelts, K. (Eds.), Global Geological Record of Lake Basins, vol. 1. Cambridge University Press, pp. xvii–xxxiii.
Goossens, H., Duren, R.R., de Leeuw, J.W., Schenck, P.A., 1989. Lipids and their mode of occurrence in bacteria and sediments-2. Lipids in the sediment of a stratified, freshwater lake. Org. Geochem. 14, 27–41.
Goad, L.J., Holz, G.G., Beach, D.H., 1983. Identification of (24S)-24-methylcholesta-5, 22-dien-3β-ol as the major sterol of a marine cryptophyte and a marine haptophyte. Phytochemistry 22, 475–476.
Grice, K., Klein Breteler, W.C.M., Schouten, S., Grossi, V., de Leeuw, J.W., Sinninghe Damsté, J.S., 1998. Effects of zooplankton herbivory on biomarker proxy records. Paleoceanography 13, 686–693.
Hackley, P.C., Fishman, N., Wu, T., 2016. Organic petrology and geochemistry of mudrocks from the lacustrine Lucaogou Formation, Santanghu Basin, northwest China: Application to lake basin evolution. Int. J. Coal Geol. 168, 20–34.
Hall, P.B., Douglas, A.G., 1983. The distribution of cyclic alkanes in two lacustrine deposits. In: Bjorøy, M., et al. (Eds.), Advances in Organic Geochemistry. J. Wiley and Sons, New York, pp. 576–587.
Hakimi, M.H., Ahmed, A.F., 2016. Organic-geochemistry characterization of the Paleogene to Neogene source rocks in the Sayhut subbasin, Gulf of Aden Basin, with emphasis on organic-matter input and petroleum-generation potential. AAPG (Am. Assoc. Pet. Geol.) Bull. 100, 1749–1774.
Hanson, A.D., Zhang, S.C., Moldowan, J.M., Liang, D.G., Zhang, B.M., 2000. Molecular organic geochemistry of the Tarim Basin, Northwest China. AAPG (Am. Assoc. Pet. Geol.) Bull. 84, 1109–1128.
Hanson, A.D., Ritts, B.D., Zinniker, D., Moldowan, J.M., Biffi, U., 2001. Upper Oligocene lacustrine source rocks and petroleum systems of the northern Qaidam basin, northwest China. AAPG (Am. Assoc. Pet. Geol.) Bull. 85, 601–619.
Hayes, J.M., 1993. Factors controlling ^{13}C contents of sedimentary organic compounds: Principles and evidence. Mar. Geol. 113, 111–125.
Horsfield, B., Curry, D.J., Bohacs, K., Littke, R., Rullkötter, J., Schenk, H.J., Radke, M., Schaefer, R.G., Carroll, A.R., Isaksen, G., Witte, E.G., 1994. Organic geochemistry of freshwater and alkaline lacustrine sediments in the Green River Formation of the Washakie Basin, Wyoming, USA. Org. Geochem. 22, 415–440.
Huang, D.F., Li, J.C., Zhang, D.J., 1990. Maturation sequence of continental crude oils in hydrocarbon basins in China and its significance. Org. Geochem. 16, 521–529.
Huang, W.Y., Meinshein, W.G., 1979. Sterols as ecological indicators. Geochem. Cosmochim. Acta 43, 739–745.
Ishiwatari, R., Uzaki, M., 1987. Diagenetic changes lignin compounds in a more than 0.6 million-year-old lacustriue sediment (Lake Biwa, Japan). Geochem. Cosmochim. Acta 51, 321–328.
Jasper, J.P., Gagosian, B.B., 1990. The sources and deposition of organic matter in the Late Quaternary Pigmy Basin, Gulf of Mexico. Geochem. Cosmochim. Acta 54, 1117–1132.
Jiang, Q.C., Ma, Y.S., Shen, Y.C., Guo, R.T., Gao, X.Q., Liu, B., Cui, J., Wu, K.Y., 2019. High-frequency redox variations of the Eocene cyclic lacustrine sediments in the Yingxi area, western Qaidam Basin, China. J. Asian Earth Sci. 174, 135–151.
Jones, R.W., Demaison, G.J., 1982. Organic Facies - stratigraphic concepts and exploration tool. In: Saldivar-Sali, A. (Ed.), Proceedings of the Second ASCOPE Conference and Exhibition, Manilla. Asean Council on Petroleum, pp. 51–68.
Kodner, R.B., Pearson, A., Summons, R.E., Knoll, A.H., 2008. Sterols in red and green algae: quantification, phylogeny, and relevance for the interpretation of geologic steranes. Geobiology 6, 411–420.
Liao, Z., Lu, L., Jiang, N., Xia, F., Song, F., Zhou, Y., Li, S., Zhang, Z., 1987. Carboniferous and Permian in the western part of the east Tianshan Mountains. Eleventh Congress of Carboniferous Stratigraphy and Geology. Guid. Excursions 4, 50.
Liu, B., Bechtel, A., Sachsenhofer, R.F., Gross, D., Gratzer, R., Chen, X., 2017. Depositional environment of oil shale within the second member of Permian Lucaogou Formation in the Santanghu Basin, Northwest China. Int. J. Coal Geol. 175, 10–25.
Liu, B., Bechtel, A., Gross, D., Fu, X., Li, X., Sachsenhofer, R.F., 2018. Middle Permian environmental changes and shale oil potential evidenced by high-resolution organic petrology, geochemistry and mineral composition of the sediments in the Santanghu Basin, Northwest China. Int. J. Coal Geol. 185, 119–137.
Liu, D.D., Fan, Q.Q., Zhang, C., Gao, Y., Du, W., Song, Y., Zhang, Z.Y., Luo, Q., Jiang, Z. X., Huang, Z.X., 2022. Paleoenvironment evolution of the Permian Lucaogou Formation in the southern Junggar Basin, NW China. Palaeogeogr. Palaeoclimatol. Palaeoecol. 603, 1–14.
Liu, B., Song, Y., Zhu, K., Su, P., Ye, X., Zhao, W.C., 2020. Mineralogy and element geochemistry of salinized lacustrine organic-rich shale in the Middle Permian Santanghu Basin: Implications for paleoenvironment, provenance, tectonic setting and shale oil potential. Mar. Petrol. Geol. 120, 1–13.
Liu, C., Liu, K.Y., Wang, X.Q., Zhu, R.K., Wu, L.Y., Xu, X.Y., 2019a. Chemo-sedimentary facies analysis of fine-grained sediment formations: An example from the Lucaogou Fm in the Jimusaer sag, Junggar Basin, NW China. Mar. Petrol. Geol. 110, 388–402.
Liu, C., Liu, K.Y., Wang, X.Q., Wu, L.Y., Fan, Y.C., 2019b. Chemostratigraphy and sedimentary facies analysis of the Permian Lucaogou Formation in the Jimusaer Sag, Junggar Basin, NW China: Implications for tight oil exploration. J. Asian Earth Sci. 178, 96–111.
Manzi, V., Roveri, M., Gennari, R., Bertini, A., Biffi, U., Giunta, S., Iaccarino, S.M., Lanci, L., Lugli, S., Negri, A., Riva, A., Rossi, M.E., Taviani, M., 2007. The deep-water counterpart of the Messinian Lower Evaporites in the Apennine foredeep: the Fanantello section (Northern Apennines, Italy). Palaeogeogr. Palaeoclimatol. Palaeoecol. 251, 470–499.
Méjanelle, L., Lòpez, J.F., Gunde-Cimerman, N., Grimalt, J.O., 2000. Sterols of melanized fungi from hypersaline environments. Org. Geochem. 31, 1031–1040.

Mello, M.R., Telnaes, N., Gaglianone, P.C., Chicarelli, M.I., Brassell, S.C., Maxwell, J.R., 1988. Organic geochemical characterization of depositional paleoenvironments in Brazilian marginal basins. Org. Geochem. 13, 31–46.
Meng, Z.Y., Liu, Y.Q., Jiao, X., Ma, L.T., Zhou, D.W., Li, H., Cao, Q., Zhao, M.R., Yang, Y. Y., 2022. Petrological and organic geochemical characteristics of the Permian Lucaogou Formation in the Jimsar Sag, Junggar Basin, NW China: Implications on the relationship between hydrocarbon accumulation and volcanic-hydrothermal activities. J. Petrol. Sci. Eng. 210, 1–17.
Meyers, P.A., Ishiwatari, R., 1993. Lacustrine organic geochemistry-an overview of indicators of organic matter sources and diagenesis in lake sediments. Org. Geochem. 20, 867–900.
Meyers, P.A., 1997. Organic geochemical proxies of paleooceanographic, paleolimnlogic, and paleoclimatic processes. Org. Geochem. 27, 213–250.
Meyers, P.A., 2003. Applications of organic geochemistry to paleolimnological reconstructions: a summary of examples from the Laurentian Great Lakes. Org. Geochem. 34, 261–289.
Mitchum Jr., R.M., Van Wagoner, J.C., 1991. High-frequency sequences and their stacking patterns: sequence-stratigraphic evidence of high-frequency cycles. Sediment. Geol. 70, 131–160.
Moore, R.C., 1949. Meaning of Facies, vol.39. The Geological Society of American, Memior, pp. 1–34.
Moldowan, J.M., Seifert, W.K., Gallegos, E.J., 1985. Relationship between petroleum composition and depositional environment of petroleum source rocks. AAPG (Am. Assoc. Pet. Geol.) Bull. 69, 1255–1268.
Moldowan, J.M., Sundararaman, P., Schoell, M., 1986. Sensitivity of biomarker properties to depositional environment and/or source input in the Lower Toarcian of S. W. Germany. Org. Geochem. 10, 915–926.
Obrist-Farner, J., Yang, W., 2016. Implications of loess and fluvial deposits on paleoclimatic conditions during an icehouse–hothouse transition, Capitanian upper Quanzijie low-order cycle, Bogda Mountains, NW China. Palaeogeogr. Palaeoclimatol. Palaeoecol. 441, 959–981.
Olariu, C., Zhang, Z.J., Zhou, C.M., Yuan, X.J., Steel, R., Chen, S., Zhang, J.Y., Cheng, D. W., 2022. Conglomerate to mudstone lacustrine cycles revealed in Junggar Basin, Northwest China: Middle Permian Lucaogou and Jingjingzigou formations. Mar. Petrol. Geol. 136, 1–20.
O'Leary, M.H., 1988. Carbon isotopes in photosynthesis. Bioscience 38, 328–336.
Ourisson, G., Albrecht, P., Rohmer, M., 1979. The hopanoids: palaeo-chemistry and biochemistry of a group of natural products. Pure Appl. Chem. 51, 709–729.
Ourisson, G., Albrecht, P., 1992. Hopanoids. 1. Geohopanoids: The Most Abundant Natural Products on Earth. Accounts Chem. Res. 25, 398–402.
Peters, K.E., Moldowan, J.M., Sundararaman, P., 1990. Effects of hydrous pyrolysis on biomarker thermal maturity parameters: Monterey Phosphatic and Siliceous Members. Org. Geochem. 15, 249–265.
Peters, K.E., Moldowan, J.M., 1991. Effects of source, thermal maturity, and biodegradation on the distribution and isomerization of homohopanes in petroleum. Org. Geochem. 17, 47–61.
Peters, K.E., Moldowan, J.M., 1993. The biomarker guide. Interpreting Geochemical Fossils in Petroleum and Ancient Sediments, first ed. Prentice Hall, Englewood, Cliffs, New Jersey.
Peters, K.E., Walter, M.M., Moldowan, J.M., 2005. The Biomarker Guide. Biomarkers and Isotopes in Petroleum Exploration and Earth History, second ed. Cambridge University Press, UK.
Powell, A.J., 1987. Thanetian dinoflagellate cyst biostratigraphy and quantitative palynostratigraphy of the Andrew Field, Central North Sea. In: British Micropalaeontological Society Meeting Micropalaeontology, Palynology, and Petroleum Exploration, on- and Offshore Europe. University of Aberdeen.
Prahl, F.G., Bennett, J.T., Carpenter, R., 1980. The early diagenesis of aliphatic hydrocarbons and organic matter in sedimentary particulates from Dabob Bay, Washington. Geochem. Cosmochim. Acta 44, 1967–1976.
Prahl, F.G., Ertel, J.R., Goni, M.A., Sparow, M.A., Eversmeyer, B., 1994. Terrestrial organic carbon contributions to sediments on the Washington margin. Geochem. Cosmochim. Acta 58, 3035–3048.
Qiu, Z., Tao, H.F., Zou, C.N., Wang, H.Y., Ji, H.J., Zhou, S.X., 2016. Lithofacies and organic geochemistry of the Middle Permian Lucaogou Formation in the Jimusar Sag of the Junggar Basin, NW China. J. Petrol. Sci. Eng. 140, 97–107.
Rieley, G., Collier, R.J., Jones, D.M., Eglintion, G., 1991. The biogeochemistry of Ellesmere Lake, U. K. - I: Source correlation of leaf wax inputs to the sedimentary record. Org. Chem. 17, 901–912.
Ritts, B.D., Hanson, A.D., Zinniker, D., Moldowan, J.M., 1999. Lower-Middle Jurassic nonmarine source rocks and petroleum systems of the northern Qaidam Basin, northwest China. AAPG (Am. Assoc. Pet. Geol.) Bull. 83, 1980–2005.
Rohmer, M., Bisseret, P., Neunlist, S., 1992. The hopanoids, prokaryotic triterpenoids and precursors of ubiquitous molecular fossils. In: Moldowan, J.M., Albrecht, P., Philp, R.P. (Eds.), Biological Markers in Sediments and Petroleum: A Tribute to Wolfgang K. Seifert. Prentice Hall, Englewood Cliffs, New Jersy, pp. 1–17.
Rullkötter, J., Marzi, R., 1988. Natural and artificial maturation of biological markers in a Toarcian shale from northern Germany. Org. Geochem. 13, 639–645.
Sachsenhofer, R.F., Bechtel, A., Kuffner, T., Rainer, T., Gratzer, R., Sauer, R., Sperl, H., 2006. Depositional environment and source potential of Jurassic coal-bearing sediments (Gresten Formation; Höflein gas/condensate field; Austria). Petrol. Geosci. 12, 99–114.
Scalan, R.S., Smith, J.E., 1970. An improved measure of the odd-to-even predominance in the normal alkanes of sediment extracts and petroleum. Geochem. Cosmochim. Acta 34, 611–620.
Scotese, C.R., 2014. Atlas of Permo-Carboniferous Paleogeographic Maps (Mollweide Projection), Maps 53-64. In: PALEOMAP PaleoAtlas for ArcGIS the Late Paleozoic, vol. 4. PALEOMAP Project, Evanston, IL.
Seifert, W.K., Moldowan, J.M., 1978. Applications of steranes, terpanes and monoaromatics to the maturation, migration and source of crude oils. Geochem. Cosmochim. Acta 42, 77–95.
Seifert, W.K., Moldowan, J.M., 1986. Use of biological markers in petroleum exploration. Methods Geochem. Geophys. 24, 261–290.
Sepúlveda, J., Wendler, J., Leiderb, A., Kuss, H.J., Summons, R.E., Hinrichs, K.U., 2009. Molecular isotopic evidence of environmental and ecological changes across the Cenomanian–Turonian boundary in the Levant Platform of central Jordan. Org. Geochem. 40, 553–568.
Sinninghe Damsté, J.S., Kenig, F., Koopmans, M.P., Köster, J., Schouten, S., Hayes, J.M., de Leeuw, J.W., 1995. Evidence for gammacerane as an indicator of water-column stratification. Geochem. Cosmochim. Acta 59, 1895–1900.
Slatt, R.M., Rodriguez, N.D., 2012. Comparative sequence stratigraphy and organic geochemistry of gas shale: Commonality or coincidence? J. Nat. Gas Sci. Eng. 8, 68–84.
Słowakiewicz, M., Tucker, M.E., Perri, E., Pancost, R.D., 2015. Nearshore euxinia in the photic zone of an ancient sea. Palaeogeogr. Palaeoclimatol. Palaeoecol. 426, 242–259.
Słowakiewicz, M., Tucker, M.E., Hindenberg, K., Mawson, M., Idiz, E.F., Pancost, R.D., 2016. Nearshore euxinia in the photic zone of an ancient sea: Part II – Thebigger picture and implications for understanding ocean anoxia. Palaeogeogr. Palaeoclimatol. Palaeoecol. 461, 432–448.
Su, Y., Zha, M., Ding, X.J., Qu, J.X., Gao, C.H., Jin, J.H., Iglauer, S., 2019. Petrographic, palynologic and geochemical characteristics of source rocks of the Permian Lucaogou formation in Jimsar Sag, Junggar Basin, NW China: Origin of organic matter input and depositional environments. J. Petrol. Sci. Eng. 183, 1–16.
Tang, Y., Hou, Z.S., Wang, X.T., Wang, T., Wu, Q., Shen, B.H., Wang, W.Q., Zhang, H., Cao, J., Zhang, S.C., Zhang, B., Wang, X.D., Shen, S.Z., 2022. Progress of the Carboniferous and Permian stratigraphic framework and correlation of the Junggar Basin, Xinjiang, Northwest China. Geol. Rev. 68, 386–407 (in Chinese with English Abstract).
Tao, H.F., Qiu, Z., Qu, Y.Q., Liu, J., Qin, Z., Xie, Z.B., Qiu, J.L., Liu, B., 2022. Geochemistry of Middle Permian lacustrine shales in the Jimusar Sag, Junggar Basin, NW China: Implications for hydrothermal activity and organic matter enrichment. J. Asian Earth Sci. 232, 1–13.
Ten Haven, H.L., de Leeuw, J.W., Rullkötter, J., Sinninghe Damste, J.S., 1987. Restricted utility of the pristane/phytane ratio as a palaeoenvironmental indicator. Nature 330, 641–643.
Tissot, B.P., Welte, D.H., 1984. Petroleum Formation and Occurrence: A New Approach to Oil and Gas Exploration. Springer-Verlag, New York.
Thomas, S.G., Tabor, N.J., Yang, W., Myers, T.S., Yang, Y., Wang, D., 2011. Paleosol stratigraphy across the Permian-Triassic boundary, Bogda Mountains, NW China: implications for palaeoenvironmental transition through earth's largest mass extinction. Palaeogeogr. Palaeoclimatol. Palaeoecol. 308, 41–64.
Trask, P.O., 1939. Organic content of recent marine sediments. In: Trask, P.O. (Ed.), Recent Marine Sediments. American Association of Petroleum Geologists, Tulsa.
Tyson, R.V., 1995. Sedimentary Organic Matter, first ed. Chapman and Hall, London.
Volkman, J.K., Maxwell, J.R., 1986. Acyclic isoprenoids as biological markers. In: Johns, R.B. (Ed.), Biological Markers in the Sedimentary Record. Elsevier, Amsterdam, pp. 1–42.
Volkman, J.K., 1986. A review of sterol markers for marine and terrigenous organic matter. Org. Geochem. 9, 83–99.
Volkman, J.K., 1988. Biological marker compounds as indicators of the depositional environments of petroleum source rocks. In: Fleet, A.J., Kelts, K., Talbot, M.R. (Eds.), Lacustrine Petroleum Source Rocks. Blackwell, London, pp. 103–122.
Volkman, J.K., Barrett, S.M., Blackburn, S.I., Mansour, M.P., Sikes, E.L., Gelin, F., 1998. Microalgal biomarkers: A review of recent research developments. Org. Geochem. 29, 1163–1179.
Volkman, J.K., 2003. Sterols in microorganisms. Appl. Microbiol. Biotechnol. 60, 495–506.
Volkman, J.K., 2005. Sterols and other triterpenoids: source specificity and evolution of biosynthetic pathways. Org. Geochem. 36, 139–159.
Wang, J., Cao, Y.C., Wang, X.T., Liu, K.Y., Wang, Z.K., Xu, Q.S., 2018. Sedimentological constraints on the initial uplift of the West Bogda Mountains in Mid-Permian. Sci. Rep. 8, 1–14.
Wu, Q., Ramezani, J., Zhang, H., Wang, J., Zeng, F.G., Zhang, Y.C., Liu, F., Chen, J., Cai, Y.F., Hou, Z.S., Liu, C., Yang, W., Henderson, C.M., Shen, S.Z., 2021. Highprecision U-Pb age constraints on the Permian floral turnovers, paleoclimate change, and tectonics of the North China block. Geology 49, 677–681.
XBGMR (Xinjiang Bureau of Geology and Mineral Resources), 1993. Regional Geology of Xinjiang Uygur Autonomous Region. Geological Memoirs, Series 1, No. 32. Geological Publishing House, Ministry of Geology and Mineral Resources of China, Beijing (in Chinese).
Yang, W., Liu, Y., Feng, Q., Lin, J., Zhou, D., Wang, D., 2007. Sedimentary evidence of Early-Late Permian mid–latitude continental climate variability, southern Bogda Mountains, NW China. Palaeogeography, Palaeoclimatolology. Palaeoecology 252, 239–258.
Yang, W., Feng, Q., Liu, Y., Tabor, N., Miggins, D., Crowley, J.L., Lin, J., Thomas, S., 2010. Depositional environments and cyclo- and chronostratigraphy of uppermost Carboniferous-Lower Triassic fluvial-lacustrine deposits, southern Bogda Mountains, NW China - A terrestrial paleoclimatic record of mid-latitude NE Pangea. Global Planet. Change 73, 15–113.

Yang, W., 2008. Depositional systems analysis within a seismic sequence stratigraphic framework, Turpan–Hami basin. Internal Report. Tu-Ha Petroleum Bureau 49.
Yang, W., Crowley, J.L., Obrist-Farner, J., Tabor, N.J., Feng, Q., Liu, Y.Q., 2013. A marine back-arc origin for the Upper Carboniferous basement of intracontinental greater Turpan-Junggar basin - Volcanic, sedimentary, and geochronologic evidence from southern Bogda Mountains. Geological Society of America Annual Meeting 45 (1).
Yang, Y.Q., Qiu, L.W., Wan, M., Jia, X.Y., Cao, Y.C., Lei, D.W., Qu, C.S., 2019. Depositional model for a salinized lacustrine basin: The Permian Lucaogou Formation, Jimsar Sag, Junggar Basin, NW China. J. Asian Earth Sci. 178, 81–95.
Yang, W., Wan, M.L., Crowley, J.L., Wang, J., Luo, X.R., Tabor, N., Angielczyk, K.D., Gastaldo, R., Geissman, J., Liu, F., Roopnarine, P., Sidor, C.A., 2021. Paleoenvironmental and paleoclimatic evolution and cyclo- and chrono-stratigraphy of upper Permian–Lower Triassic fluvial-lacustrine deposits in Bogda Mountains, NW China — Implications for diachronous plant evolution across the Permian–Triassic boundary. Earth Sci. Rev. 222, 1–39.
Zhan, X., 2019. Paleoenvironment and paleoclimate of NE Pangea in early Permian-linking chemo- and cyclo-stratigraphy. Doctoral Dissertations 2856, pp. 1–127.
Zhang, X., 1981. Regional Stratigraphic Chart of Northwestern China, Branch of Xinjian Uygur Autonomous Region. Geological Publishing House, Beijing, p. 496 pp. (in Chinese).
Zhang, M.M., Li, Z., 2018. The lithofacies and reservoir characteristics of the fine-grained sedimentary rocks of the Permian Lucaogou Formation at the northern foot of Bogda Mountains, Junggar Basin (NW China). J. Petrol. Sci. Eng. 170, 21–39.
Zhang, J.Y., Liu, G.D., Cao, Z., Tao, S.Z., Felix, M., Kong, Y.H., Zhang, Y.Y., 2019. Characteristics and formation mechanism of multi-source mixed sedimentary rocks in a saline lake, a case study of the Permian Lucaogou Formation in the Jimusaer Sag, northwest China. Mar. Petrol. Geol. 102, 704–724.
Zhang, S.H., Liu, C.Y., Liang, H., Jia, L.B., Bai, J.K., Zhang, L., Wang, J.Q., 2021. Mineralogical composition and organic matter characteristics of lacustrine fine-grained volcanic-hydrothermal sedimentary rocks: A data-driven analytics for the second member of Permian Lucaogou Formation, Santanghu Basin, NW China. Mar. Petrol. Geol. 126, 1–15.
Zhao, Y., Wu, F.L., Fang, X.M., Yang, Y.B., 2015. Topsoil C/N ratios in the Qilian Mountains area: Implications for the use of subaqueous sediment C/N ratios in paleo-environmental reconstructions to indicate organic sources. Palaeogeogr. Palaeoclimatol. Palaeoecol. 426, 1–9.